Monthly Notices
of the
ROYAL ASTRONOMICAL SOCIETY

MNRAS **450,** 2764–2783 (2015) doi:10.1093/mnras/stv528

Spectroscopic survey of *Kepler* stars.★ I. HERMES/Mercator observations of A- and F-type stars

E. Niemczura,[1]† S. J. Murphy,[2,3] B. Smalley,[4] K. Uytterhoeven,[5,6] A. Pigulski,[1] H. Lehmann,[7] D. M. Bowman,[8] G. Catanzaro,[9] E. van Aarle,[10] S. Bloemen,[11] M. Briquet,[12] P. De Cat,[13] D. Drobek,[1] L. Eyer,[14] J. F. S. Gameiro,[15] N. Gorlova,[10] K. Kamiński,[16] P. Lampens,[13] P. Marcos-Arenal,[10] P. I. Pápics,[10] B. Vandenbussche,[10] H. Van Winckel,[10] M. Stęślicki[17] and M. Fagas[16]

Affiliations are listed at the end of the paper

Accepted 2015 March 6. Received 2015 March 5; in original form 2014 October 28

ABSTRACT

The *Kepler* space mission provided near-continuous and high-precision photometry of about 207 000 stars, which can be used for asteroseismology. However, for successful seismic modeling it is equally important to have accurate stellar physical parameters. Therefore, supplementary ground-based data are needed. We report the results of the analysis of high-resolution spectroscopic data of A- and F-type stars from the *Kepler* field, which were obtained with the HERMES spectrograph on the Mercator telescope. We determined spectral types, atmospheric parameters and chemical abundances for a sample of 117 stars. Hydrogen Balmer, Fe I, and Fe II lines were used to derive effective temperatures, surface gravities, and microturbulent velocities. We determined chemical abundances and projected rotational velocities using a spectrum synthesis technique. The atmospheric parameters obtained were compared with those from the *Kepler Input Catalogue* (KIC), confirming that the KIC effective temperatures are underestimated for A stars. Effective temperatures calculated by spectral energy distribution fitting are in good agreement with those determined from the spectral line analysis. The analysed sample comprises stars with approximately solar chemical abundances, as well as chemically peculiar stars of the Am, Ap, and λ Boo types. The distribution of the projected rotational velocity, $v \sin i$, is typical for A and F stars and ranges from 8 to about 280 km s^{-1}, with a mean of 134 km s^{-1}.

Key words: stars: abundances – stars: chemically peculiar – stars: general – stars: rotation.

1 INTRODUCTION

The NASA space mission *Kepler* was successfully launched on 2009 March 7. The main scientific goal of the mission was to discover Earth-sized planets around Sun-like stars (Borucki et al. 2010). During 2013 May the satellite lost the second of its four reaction wheels (the first one failed in 2012 July), preventing further observation of the original field. Nevertheless, during the four years of near-continuous data collection, *Kepler* produced photometric time series of an exceptional precision of a few parts per million, which provide a unique and excellent data base for studying variability due to pulsations in thousands of stars across the Hertzsprung–Russell (H-R) diagram (Kjeldsen et al. 2010).

Asteroseismology is the only way to probe the internal structure of stars and significantly improve our understanding of stellar evolution. It provides direct tests of the modelling of processes taking place in stellar interiors, such as diffusion, transport of angular momentum (Mosser et al. 2012; Marques et al. 2013), convective overshooting, mechanisms driving pulsations (e.g. Moravveji et al. 2012; Antoci et al. 2014), and the value of the mixing-length parameter in stars of different effective temperatures (Trampedach &

★Based on observations made with the Mercator Telescope, operated on the island of La Palma by the Flemish Community, at the Spanish Observatorio del Roque de los Muchachos of the Instituto de Astrofsica de Canarias. Based on observations obtained with the HERMES spectrograph, which is supported by the Fund for Scientific Research of Flanders (FWO), Belgium, the Research Council of K.U.Leuven, Belgium, the Fonds National Recherches Scientific (FNRS), Belgium, the Royal Observatory of Belgium, the Observatoire de Genve, Switzerland and the Thringer Landessternwarte Tautenburg, Germany.

†E-mail: eniem@astro.uni.wroc.pl

© 2015 The Authors
Published by Oxford University Press on behalf of the Royal Astronomical Society

Downloaded from http://mnras.oxfordjournals.org/ at The Library on May 18, 2016

Stein 2011; Bonaca et al. 2012). The key ingredients for an asteroseismic study are precise pulsation frequencies, mode identification, and strong constraints on atmospheric parameters, such as effective temperature $T_{\rm eff}$, surface gravity $\log g$, chemical abundances, and rotational velocity $v \sin i$. Accurate values of the pulsation frequencies are provided by the ultra-precise *Kepler* photometry. The accuracy of atmospheric parameters available from the *Kepler Input Catalogue* (KIC) (Brown et al. 2011) is generally too low for asteroseismic modelling, particularly for stars of spectral types earlier than F0 (Huber et al. 2014, hereafter H2014). Also, information on the stellar chemical composition and rotational velocity is lacking. Therefore, high-resolution spectra, which offer a wide range of information, are needed to fully characterize *Kepler* targets (Uytterhoeven 2014).

For more than a 1000 *Kepler* stars high- and medium-resolution spectra have been collected (Uytterhoeven et al. 2010). These observations are summarized in the *Kepler Asteroseismic Science Operations Center* (KASOC) data base.[1] In this paper, we focus on the analysis of high-resolution spectra of main-sequence A- and F-type stars. The main groups of pulsators among these objects are δ Scuti, γ Doradus, and γ Dor/δ Sct hybrid stars. The δ Sct stars are main-sequence or evolved stars situated in the classical instability strip. They pulsate in low-order radial and non-radial pressure modes (p-modes) with typical frequencies of 5 to 50 d^{-1} (see reviews by Breger 2000; Handler 2009; Balona 2014). The γ Dor stars are pulsating variables with spectral types A7–F5 that are on or close to the main sequence and pulsate in high-order gravity modes (g-modes) with typical frequencies of 0.3 to 3 d^{-1} (Kaye et al. 1999). The instability strip for γ Dor stars partly overlaps with the δ Sct instability strip. The γ Dor variables are of particular interest in asteroseismology, as their g-mode pulsations probe the deep interiors of these stars, reaching their convective cores. Additionally, these pulsators occupy a region in the H-R diagram where γ Dor-like g-mode pulsations, δ Sct-like p-mode pulsations and possibly solar-like oscillations can co-exist in a single star. This overlap means that some individual objects show g-mode as well as p-mode pulsations. These hybrid variables permit simultaneous probing of two distinct regions of the interior: the deep layers between the convective core and the envelope, where the g-modes propagate, and the outer layers of the envelope where the p-modes propagate (Kurtz et al. 2014; Saio et al. 2015). Therefore, hybrid stars are key objects for testing stellar models with seismic techniques.

Grigahcène et al. (2010) found that the hybrid stars in the *Kepler* field are spread over the entire δ Sct and γ Dor instability domains. The analysis of *Kepler* data and KIC parameters for 750 A and F stars presented by Uytterhoeven et al. (2011) confirms this result. They found that 23 per cent of their sample of A and F objects shows both δ Sct pulsations and low-frequency variations. Balona & Dziembowski (2011) analysed observations of 1568 δ Sct pulsators taken from the *Kepler* archive and identified a group of δ Sct stars with low-frequency peaks similar to those characteristic for γ Dor stars. Contrary to the results of Uytterhoeven et al. (2011) and Grigahcène et al. (2010), these variables are located in the same region of the H-R diagram as the ground-based γ Dor pulsators and none is found in the δ Sct instability domain. The low frequencies are observed in the hotter stars, but their origin is not clear (Balona 2014). A high-resolution spectroscopic analysis by Tkachenko et al. (2013b) found each of their 38 γ Dor stars to lie within the γ Dor instability strip. Accurate stellar atmospheric parameters are clearly required to place γ Dor/δ Sct hybrids unambiguously in the H-R diagram.

This paper is organized as follows: in Section 2, we describe observational data used in the analysis. Details of the spectral classification methods are given in Section 3. In Section 4, we present all the methods applied for determining the atmospheric parameters of the investigated objects, the sources of possible errors, and discuss consistency of the results obtained from different approaches. The distribution of rotational velocities is presented and discussed in Section 5. The derived abundances of elements, their correlation with the other parameters and a sample of chemically peculiar (CP) stars are discussed in Section 6. Positions of the analysed stars in the $\log T_{\rm eff}$ – $\log g$ diagram, conclusions and future prospects are given in Section 7.

2 SPECTROSCOPIC SURVEYS OF *KEPLER* STARS

High-resolution spectra were collected for several hundred stars located in the *Kepler* field of view. Most of these spectra were obtained by échelle spectrographs attached to the Mercator Telescope,[2] Nordic Optical Telescope[3] (NOT), Tautenburg 2-m Alfred-Jensch Telescope[4] (TLS), Bernard Lyot Telescope[5] and the Canada-France-Hawaii Telescope[6] (CFHT).

In this paper we analyse high-resolution spectra taken with the cross-dispersed, fibre-fed échelle spectrograph HERMES (High Efficiency and Resolution Mercator Échelle Spectrograph; Raskin et al. 2011) attached to the 1.2-m Mercator Telescope located on La Palma (Canary Islands, Spain). The spectra have a resolving power $R \sim 85\,000$ and cover the spectral range from 3770 to 9000 Å. The typical signal-to-noise (S/N) ratio for an individual spectrum at 5500 Å is 80–100. The spectra have been reduced with a dedicated pipeline,[7] which includes bias subtraction, extraction of scattered light produced by the optical system, cosmic ray filtering, division by a normalized flat-field, wavelength calibration by a ThArNe lamp and order merging. The normalization to the continuum was performed manually by using the standard IRAF[8] procedure *continuum*. Most of the stars in our sample have $v \sin i > 40$ km s^{-1}. The spectra of rapid rotators are very difficult to normalize correctly in spectral regions rich in blended lines, e.g. for $\lambda < 4100$ Å. For this reason, we checked the quality of our normalization by fitting synthetic spectra to all Balmer lines in the spectrum of each star. If the spectrum has been normalized correctly, all hydrogen lines can be fitted satisfactorily with the same $T_{\rm eff}$. The process of normalization is otherwise repeated. For the few stars for which we have more than one spectrum, we analysed the averaged spectrum. The averaging process is applied after normalization and forms an additional test of the quality of the normalization process.

The data analysed in this paper were collected in spectroscopic surveys carried out in the years 2010 to 2012 (Table 1). Table 2 lists the analysed stars and gives their KIC numbers, dates of the observations, number of spectra, visual (V) magnitudes, and spectral types from the literature and determined in this paper. We also

[1] http://kasoc.phys.au.dk/

[2] http://www.mercator.iac.es
[3] http://www.not.iac.es/
[4] http://www.tls-tautenburg.de/TLS
[5] http://www.tbl.omp.eu/
[6] http://www.cfht.hawaii.edu/
[7] http://hermes-as.oma.be/
[8] Image Reduction and Analysis Facility, http://iraf.noao.edu/

Downloaded from http://mnras.oxfordjournals.org/ at The Library on May 18, 2016

Table 1. HERMES spectroscopic surveys of *Kepler* stars.

Observation dates	Primary investigator	Observers
2010 May–Sept.	M. Briquet	KU Leuven observers[a]
2011 July	E. Niemczura	D. Drobek
2011 Sept.	E. Niemczura	J. F. S. Gameiro
2012 July	K. Uytterhoeven	E. Niemczura
2012 August	P. De Cat	P. I. Pápics
2012 Sept.	P. De Cat	P. M. Arenal

Notes. [a]E. Van Aarle, S. Bloemen, N. Gorlova, P. Lampens, H. Van Winckel, B. Vandenbussche.

provide notes on chemical peculiarity, binarity and pulsation characteristics. CP stars in our sample were identified in the process of spectroscopic classification and confirmed by the detailed spectroscopic analysis afterwards. Twenty stars were found to be double-lined spectroscopic binaries (SB2) and the atmospheric parameters of these stars will be presented in a separate paper (Catanzaro et al., in preparation).

The results of the spectroscopic analysis of stars observed with the other telescopes will be presented in a forthcoming paper (Niemczura et al., in preparation).

3 SPECTRAL CLASSIFICATION

Stellar spectral classification in the Morgan–Keenan (MK) system involves determining the luminosity class and spectral type for a given star by comparing its spectrum with spectra of standards (Gray & Corbally 2009). The spectral type in A stars is determined mainly from three spectral features: (i) hydrogen lines, (ii) the Ca II K line, and (iii) lines of metals. In a non-peculiar star, all three features should consistently provide the same spectral type, if the correct luminosity class has been adopted. Determination of luminosity class in A stars is difficult. While the hydrogen lines are very sensitive to luminosity in early A stars, the A5 and later spectral types lose much of this sensitivity and at F0 the hydrogen lines become almost insensitive to the luminosity class. For F0, ionized lines of Fe and Ti become useful in determination of the luminosity class.

At late A spectral type, metallic (Am) stars are common. For these stars, spectral types determined from the Ca II K-line and metal lines differ by five or more subclasses. The Ca II K line is weak in their spectra and thus yields an earlier spectral type than hydrogen lines, while the metal lines are enhanced and typical for a later subtype. They are denoted as, for example, kA2hA5mF0 (IV), where k, h and m precedes the spectral type obtained from the Ca II K line, hydrogen lines and metal lines, respectively. These symbols are followed by the luminosity class. If the luminosity class is in parentheses, as it is in this example, then the star exhibits the anomalous luminosity effect (see Gray & Corbally 2009) where the violet part of the spectrum indicates a more luminous class than the blue part. Stars showing mild Am features, where there are fewer than five spectral subtypes between the Ca II K line and metal line types, are called marginal Am stars, denoted as Am:.

Most of the objects were classified as A stars, including slow, fast and very fast rotators ('s', 'n' and 'nn' added to the spectral type, respectively). The classified CP stars are of Am (17), Ap CrSrEu (1) and λ Boötis types (2). Additional, mild peculiarities were discovered in some of the stars, such as weak Ca or metal lines. Only three stars were classified as late B, with one of them appearing to be He strong (He-s). The assigned spectral classes are presented in Table 2 and some notes are provided in the comments below the table.

4 ATMOSPHERIC PARAMETERS

To perform an abundance analysis, one needs an appropriate atmospheric model of the star, which requires the effective temperature,

Table 2. Spectroscopic observations and the derived spectral classes. *N* is the number of available spectra; SpT1 indicates the spectral classification from the literature, whereas SpT2 means spectral classifications obtained in this work. Superscript ⋆ in the first column denotes the stars with additional information below the table. Additional notation for luminosity class: b – lower luminosity main-sequence star; a or a+ – higher luminosity main-sequence star; IV-V – between IV and V; IV/V – either IV or V; n – nebulous (i.e. broad-lined); s – sharp lines; nn – very rapid rotators; wk met – weak metal lines; met str – strong metal lines. In the last column additional information taken from spectra and *Kepler* data are presented: SB2 – double-lined spectroscopic binary; rot. – rotational frequency detected; bin. – orbital frequency detected; mult. – orbital frequencies of both components detected; hybrid – frequencies of γ Dor and δ Sct visible in the pulsation spectra; contamination – *Kepler* data contaminated by a nearby star; ? – our classification of variability type is uncertain. The full table is available in the electronic form.

KIC number	HERMES observations	*N*	*V* [mag]	SpT1	SpT2 (this paper)	Notes
1294756	2010 May–September	1	8.96	A2[a]	A3 IV	mult. + rot. + δ Sct
2571868	2011 July	1	8.67	A0[a]	A3 IVn	hybrid (low. ampl. γ Dor)
2694337	2010 May–September	1	10.35		F0.5 IVs	hybrid
2695344	2012 July	1	9.62	F2[a]	F2 V	SB2; γ Dor
	2012 September	1				
3230227⋆	2010 May–September	1	8.94	A5[a]	A5 IV:	SB2; ecl. bin. + δ Sct
3231985⋆	2011 September	1	9.22	A2[a]	A4 IV Ca weak (A3)	rot.
3347643	2010 May–September	1	7.69	A2[a]	A3 V an	hybrid (low. ampl. γ Dor)
3441230	2012 July	1	9.79	A2[a]	kA2hA5mF0 V Am	rot.
3656913	2012 July	1	9.81	A0[a]	kA2hA6mF0 IV Am	SB2; bin.
3850810⋆	2010 May–September	1	10.10		F1 Vs wk met (F0)	hybrid + rot.

Notes. KIC 3230227: Incorrectly normalized H lines; wings are unusable but core matches A5 IV. Metal lines indicate A5 V. KIC 3231985: Weak Ca K and Ca λ4226 line. KIC 3850810: Considerably metal weak or poorly normalized.
[a]Heckmann & Dieckvoss (1975).

Downloaded from http://mnras.oxfordjournals.org/ at The Library on May 18, 2016

Table 3. Atmospheric parameters of the investigated *Kepler* A and F stars. We present parameters derived from the KIC photometry (KIC), those obtained from spectral energy distributions (Na D & SED) and from analysis of metal and Balmer lines. The 1σ uncertainties are given for effective temperatures derived from SED fitting, and for $v\sin i$ and $\log\epsilon$(Fe) values derived from metal lines. The full table is available in the electronic form.

KIC			KIC		Na D and SED		Metal and Balmer lines				
number	$T_{\rm eff}$ [K]	$\log g$	$E(B-V)$ [mag]	$\log\epsilon$(Fe)	$E(B-V)$ [mag]	$T_{\rm eff}$ [K]	$T_{\rm eff}$ [K]	$\log g$	$\xi_{\rm t}$ [km s^{-1}]	$v\sin i$ [km s^{-1}]	$\log\epsilon$(Fe)
10263800	8573	3.89	0.09	7.44	0.01	8590 ± 210	8900 ± 200	4.0 ± 0.2	2.0 ± 0.4	230 ± 7	6.91 ± 0.15
10264728	7794	3.85	0.09	7.42	0.03	7790 ± 200	7900 ± 200	3.8 ± 0.2	1.3 ± 0.4	257 ± 8	7.59 ± 0.12
10355055	8110	3.74	0.10	7.43	0.05	8420 ± 270	8300 ± 200	3.8 ± 0.2	2.9 ± 0.4	223 ± 7	7.29 ± 0.11
10533616	8317	3.77	0.10	7.48	0.02	8260 ± 250	8200 ± 100	3.8 ± 0.2	2.0 ± 0.2	128 ± 3	7.68 ± 0.11
10549371	6973	3.95	0.06	7.12	0.06	7300 ± 170	7200 ± 100	3.8 ± 0.1	3.9 ± 0.1	71 ± 2	7.32 ± 0.09
10555142	6998	3.51	0.08	7.32	0.04	7180 ± 160	7000 ± 200	3.8 ± 0.2	2.5 ± 0.4	210 ± 5	7.45 ± 0.14
10590857	7564	3.76	0.09	7.41	0.02	7470 ± 180	7300 ± 100	4.0 ± 0.2	2.9 ± 0.2	108 ± 4	7.53 ± 0.09
10721930	8311	3.73	0.10	7.47	0.06	8480 ± 210	8200 ± 100	3.7 ± 0.1	1.7 ± 0.1	16 ± 1	7.48 ± 0.17
10977859	8052	3.93	0.06	7.65	0.01	8400 ± 250	8200 ± 100	3.7 ± 0.1	1.6 ± 0.1	65 ± 2	7.55 ± 0.16
11013201	7779	3.82	0.07	7.44	0.01	7740 ± 260	7800 ± 100	3.8 ± 0.2	1.7 ± 0.2	117 ± 2	7.71 ± 0.08

surface gravity and metallicity to be known. To determine these parameters, we applied both photometric and spectroscopic methods.

4.1 Effective temperatures from spectral energy distributions

Effective temperature can be determined from the stellar spectral energy distribution (SED). For our target stars these were constructed from the available photometry, using 2MASS (Skrutskie et al. 2006), Tycho B and V magnitudes (Høg et al. 1997), USNO-B1 R magnitudes (Monet et al. 2003), and TASS I magnitudes (Droege, Richmond & Sallman 2006), supplemented, if available, by Geneva photometry (Rufener 1999), CMC14 r' magnitudes (Evans, Irwin & Helmer 2002) and TD-1 ultraviolet flux measurements (Carnochan 1979).

SEDs can be significantly affected by interstellar reddening. We have, therefore, estimated this parameter from the interstellar Na D_2 (5889.95 Å) lines. The equivalent widths of the D_2 lines were measured and $E(B-V)$ values were obtained using the relation given by Munari & Zwitter (1997). For resolved multi-component interstellar Na D_2 lines, the equivalent widths of the individual components were measured. The total $E(B-V)$ in these cases is the sum of the reddening per component, since interstellar reddening is additive (Munari & Zwitter 1997). The SEDs were de-reddened using the analytical extinction fits of Seaton (1979) for the ultraviolet and Howarth (1983) for the optical and infrared.

Effective temperatures were determined by fitting Kurucz (1993a) model fluxes to the de-reddened SEDs. The model fluxes were convolved with photometric filter response functions. A weighted Levenberg–Marquardt non-linear least-squares fitting procedure was used to find the solution that minimized the difference between the observed and model fluxes. Since $\log g$ and metallicity [M/H] are poorly constrained by our SEDs, we fixed $\log g = 4.0$ and [M/H] $= 0.0$ dex for all of the fits. The results are given in Table 3. The uncertainties in $T_{\rm eff}$ include the formal least-squares error and adopted uncertainties in $E(B-V)$ of ± 0.02 mag, $\log g$ of ± 0.5 dex and [M/H] of ± 0.5 dex added in quadrature.

4.2 Atmospheric parameters from spectroscopy

We used atmospheric models and synthetic spectra to obtain atmospheric parameters, abundances of chemical elements and rotational velocities from the high-resolution HERMES spectra. All the necessary atmospheric models were computed with the line-blanketed, local thermodynamical equilibrium (LTE) ATLAS9 code (Kurucz 1993a). The physics of the models includes plane-parallel geometry, and hydrostatic and radiative equilibrium. Models were pre-calculated in a grid for effective temperatures between 5000 and 12 000 K with a step of 100 K, surface gravities from 2.0 to 4.6 dex with a step of 0.1 dex, and for solar metallicity. Additional models of non-solar metallicity were calculated for smaller ranges of effective temperatures and surface gravities. The synthetic spectra were computed with the ATLAS9 code (Kurucz 1993b). Both codes, ATLAS9 and SYNTHE, were ported to GNU/Linux by Sbordone (2005) and are available online.[9] The stellar line identification and the abundance analysis in the entire observed spectral range were performed on the basis of the line list from Castelli & Hubrig (2004).

We analysed the metal lines following the spectrum synthesis methodology established by Niemczura & Połubek (2006) and Niemczura, Morel & Aerts (2009). It relies on an efficient least-squares optimisation algorithm (see Bevington 1969; Takeda 1995), and is appropriate over a wide range of $v\sin i$ values. Our observed $v\sin i$ range is 8 to 283 km s^{-1}, which includes stars rotating too rapidly for equivalent width analysis to be possible due to line blending. The spectrum synthesis method allows for a simultaneous determination of various parameters influencing stellar spectra and consists of the minimization of the deviation between the theoretical and observed spectra. The synthetic spectrum depends on stellar parameters such as $T_{\rm eff}$, $\log g$, $\xi_{\rm t}$, $v\sin i$, radial velocity $v_{\rm r}$, and the relative abundances of the elements $\log\epsilon$(El), where El denotes the individual element. All atmospheric parameters are correlated. In our method, the $T_{\rm eff}$, $\log g$ and $\xi_{\rm t}$ parameters were obtained prior to the determination of abundances of chemical elements and were considered as input parameters. The remaining parameters ($\log\epsilon$(El), $v\sin i$ and $v_{\rm r}$) were determined simultaneously because they produce detectable and different spectral signatures. The $v\sin i$ values were determined by comparing the shapes of observed metal line profiles with the computed profiles, as shown by Gray (2005).

The starting values of $T_{\rm eff}$ were taken from the SED fits, and values $\log g$ came from the KIC. These parameters were then improved by using the sensitivity of Balmer lines to effective temperature and gravity, following the method proposed by Catanzaro, Leone & Dall (2004). However, hydrogen lines cease to be good indicators of $\log g$ for effective temperatures cooler than 8000 K. Therefore, for stars with lower effective temperatures, the surface gravity was initially

[9] http://wwwuser.oats.inaf.it/castelli/

Downloaded from http://mnras.oxfordjournals.org/ at The Library on May 18, 2016

assumed to be equal to 4.0 dex. We used an iterative approach to minimize the differences between observed and synthetic Hδ, Hγ and Hβ profiles (see Catanzaro et al. 2004).

The effective temperatures and surface gravities determined from Balmer lines were improved through the analysis of lines of neutral and ionized iron. In this method, we adjusted $T_{\rm eff}$, $\log g$ and $\xi_{\rm t}$ by comparing the abundances determined from Fe I and Fe II lines. The analysis was based on iron lines because they are the most numerous in our spectra. In general, we required that the abundances measured from Fe I and Fe II lines yield the same result. In the spectra of stars with lower effective temperatures, the number of Fe I lines outnumbers those of the Fe II lines. The strength of Fe I lines depends on $T_{\rm eff}$, $\xi_{\rm t}$ and metallicity [M/H], but is practically independent of $\log g$. On the other hand, the lines of Fe II are weakly sensitive to effective temperature and metallicity, but highly sensitive to gravity (Gray 2005). First, we adjusted microturbulence until we saw no correlation between iron abundances and line depths for the Fe I lines. Next, $T_{\rm eff}$ was changed until we saw no trend in the abundance versus excitation potential for the Fe I lines. Determinations of microturbulence and effective temperature are not independent, but since the influence of microturbulence on spectral lines is stronger, we adjusted this parameter first. Then, surface gravity is obtained by fitting the Fe II and Fe I lines, and by requiring the same abundances from the lines of both ions. For hotter stars, whose spectra show more Fe II than Fe I lines, the Fe II lines were used to determine $T_{\rm eff}$ and $\xi_{\rm t}$, whereas $\log g$ was derived from Balmer lines (Gray 2005). This approach is limited by stellar rotation, since line blending grows rapidly with $v\sin i$. In the spectra of rapid rotators all the lines are blended and it is impossible to use individual iron lines for $T_{\rm eff}$, $\log g$ and $\xi_{\rm t}$ determination. In such cases we assumed that the abundances obtained from Fe I and Fe II lines are the same for the correct $T_{\rm eff}$, $\log g$ and $\xi_{\rm t}$. The analysis relies on the same physics, regardless of rotation. The only difference is that for slow and moderate rotators we can use separate iron lines, including weak lines, to calculate the atmospheric parameters. For rapid rotators we are comparing iron abundances derived from broader spectral regions. Typically such regions contain many iron lines, both neutral and ionized. Of course, in such cases, stronger lines have more influence on the result.

Having derived $T_{\rm eff}$, $\log g$ and $\xi_{\rm t}$, the determination of abundances could be performed. The analysis of chemical abundances began with the selection of spectral regions suitable for abundance analysis. The length of a chosen part depended mainly on $v\sin i$. For slowly rotating stars ($v\sin i < 40$ km s^{-1}), short sections covering only one or a few blended spectral features were used. For stars with $v\sin i > 40$ km s^{-1}, we used broader spectral ranges re-normalized by comparison with theoretical spectra, if necessary. The next step was line identification in the chosen region. For rapidly rotating stars, where all lines are blended, only the most important elements producing spectral features were considered. In our method, we can take into account all elements that have lines in the chosen spectral region. Elements that have little or no influence on the spectra are included in the analysis, but no attempt is made to calculate their abundances. The stellar rotation and S/N ratio of the spectrum dictate for which elements the abundance analysis is performed.

The line list used is that of Castelli & Hubrig (2004), which is based on Kurucz's line list[10] and supplemented by additional sources. It was prepared for the analysis of CP Ap and HgMn stars, hence is suitable for the analysis of our CP stars. Each selected spectral region was analysed by the spectral synthesis method described above. We adjusted $v_{\rm r}$, $v\sin i$ and chemical abundances to minimize the difference between the calculated and observed spectra. The final solution was typically reached after 10 iterations. The iterations stopped if the values of the determined parameters remained the same within 2 per cent for three consecutive steps. In our method, chemical abundances and $v\sin i$ values were determined from many parts of the spectrum. In the final step of the analysis, we derived the average values of $v\sin i$ and abundances of all the chemical elements considered for a given star and estimated the uncertainty on the derived abundances.

In our analysis we do not take into account macroturbulence, whose influence on the line profile is degenerate with $v\sin i$. The effect of macroturbulence on F stars was discussed in detail by Fossati et al. (2011), who found that stronger lines required higher macroturbulent velocities and interpreted this as the effect of unmodelled depth-dependent velocities in the atmosphere. Since these are not observable in A stars, the required macroturbulent velocities remain uncertain, but the effect of macroturbulence is mainly limited to $v\sin i$. The other parameters can be slightly affected, especially for slowly rotating stars (Fossati et al. 2011). The $v\sin i$ values of slow rotators may be overestimated due to non-inclusion of macroturbulence. However, for $v\sin i > 50$ km s^{-1} the effect of modest (e.g. 10 km s^{-1}) macroturbulence is negligible at our resolution and S/N.

The atmospheric parameters obtained from our analysis are given in Table 3, and the abundances of analysed elements are given in Table 4.

4.3 Discussion of uncertainties

The derived atmospheric parameters and chemical abundances are influenced by errors from a number of sources. First of all, the adopted atmosphere models and synthetic spectra were calculated taking into account several simplifications, e.g. LTE, plane parallel geometry (1D), and hydrostatic equilibrium (Kurucz 1993a), instead of a 3D and non-LTE approach (e.g. Bergemann et al. 2012).

Recently, the non-LTE line formation for Fe I and Fe II for stars with $T_{\rm eff}$ between 6500 K and 8500 K and $\log g$ between 3.0 and 4.0 dex was discussed by Mashonkina (2011). In this paper, the non-LTE calculations were performed with a complete model atom, as described therein. The departures from LTE caused the depletion of total absorption in the Fe I lines and positive abundance corrections, leading to an underestimation of Fe abundance in LTE calculations. However, the corrections to LTE abundances were found to be smaller than 0.1 dex for main-sequence stars. For Fe II, the non-LTE effect was again found to be negligible, with corrections of -0.01 to -0.03 dex over the whole range of considered stellar parameters. Most stars in our sample have effective temperatures lower than 8500 K. The non-LTE correction of Fe abundances for these stars was less than 0.1 dex. Application of this correction would change $\log g$ determinations from the ionization balance of Fe I and Fe II lines. If we add non-LTE corrections to the obtained abundances of Fe I, the determined surface gravity would be higher by about 0.1 dex. However, in most of our investigated stars, high projected rotational velocities prevent us from obtaining abundances of Fe I and Fe II separately. Therefore, we did not include the non-LTE corrections in the present analysis.

Other important factors affecting spectral analysis are atomic data (Kurucz 2011), quality (resolution, S/N), wavelength range of the observed spectra and their normalization. It is quite easy to normalize the optical spectrum of an A star with $v\sin i < 40$ km s^{-1}.

[10] http://kurucz.harvard.edu/linelists.html

Downloaded from http://mnras.oxfordjournals.org/ at The Library on May 18, 2016

Table 4. Abundances of chemical elements for a sample of analysed stars (on the scale in which $\log \epsilon(\mathrm{H}) = 12$). The median value is given; standard deviations were calculated only if the number of analysed parts of a spectrum was greater than three. In other cases the average value calculated from standard deviations of other elements is given. The number of analysed parts is given in brackets. The full table is available in the electronic version.

	KIC 10263800	KIC 10264728	KIC 10355055	KIC 10533616	KIC 10549371	KIC 10555142	KIC 10590857
C	8.85 ± 0.14 (1)	8.48 ± 0.12 (2)	8.90 ± 0.12 (2)	8.38 ± 0.07 (7)	8.31 ± 0.14 (14)	8.78 ± 0.16 (5)	8.36 ± 0.19 (5)
N	–	–	–	–	8.33 ± 0.14 (1)	–	–
O	8.74 ± 0.14 (2)	9.04 ± 0.12 (1)	8.44 ± 0.12 (1)	8.92 ± 0.14 (2)	8.83 ± 0.14 (1)	–	8.91 ± 0.17 (1)
Ne	–	–	–	–	–	–	–
Na	–	6.60 ± 0.12 (1)	7.10 ± 0.12 (1)	6.89 ± 0.14 (2)	6.46 ± 0.14 (2)	6.63 ± 0.18 (1)	6.22 ± 0.17 (1)
Mg	7.68 ± 0.14 (1)	8.01 ± 0.12 (4)	7.28 ± 0.19 (3)	7.98 ± 0.10 (6)	7.56 ± 0.13 (8)	7.64 ± 0.18 (2)	7.57 ± 0.10 (4)
Al	–	–	–	–	–	–	–
Si	6.80 ± 0.14 (2)	7.94 ± 0.12 (2)	7.50 ± 0.12 (2)	7.60 ± 0.18 (5)	7.54 ± 0.20 (21)	7.52 ± 0.29 (5)	7.56 ± 0.25 (8)
P	–	–	–	–	–	–	–
S	–	–	–	–	7.32 ± 0.01 (3)	–	7.29 ± 0.17 (1)
Cl	–	–	–	–	–	–	–
K	–	–	–	–	–	–	–
Ca	6.62 ± 0.14 (2)	6.64 ± 0.12 (4)	6.61 ± 0.16 (8)	6.65 ± 0.16 (15)	6.54 ± 0.16 (25)	6.30 ± 0.23 (7)	6.67 ± 0.23 (4)
Sc	4.03 ± 0.14 (1)	3.09 ± 0.12 (3)	2.96 ± 0.11 (3)	3.10 ± 0.16 (5)	3.24 ± 0.10 (9)	2.91 ± 0.21 (4)	3.28 ± 0.13 (6)
Ti	4.43 ± 0.14 (3)	5.07 ± 0.16 (8)	5.05 ± 0.18 (9)	5.22 ± 0.17 (16)	5.06 ± 0.15 (47)	5.05 ± 0.15 (8)	5.27 ± 0.20 (14)
V	–	2.79 ± 0.12 (1)	–	–	4.43 ± 0.11 (9)	4.67 ± 0.18 (2)	–
Cr	5.46 ± 0.14 (2)	5.69 ± 0.19 (5)	5.60 ± 0.04 (6)	5.86 ± 0.09 (8)	5.53 ± 0.16 (26)	5.69 ± 0.18 (2)	5.67 ± 0.18 (16)
Mn	–	5.60 ± 0.12 (2)	5.29 ± 0.12 (1)	5.57 ± 0.14 (2)	5.35 ± 0.16 (10)	5.43 ± 0.04 (3)	5.59 ± 0.17 (2)
Fe	6.93 ± 0.15 (5)	7.54 ± 0.12 (11)	7.29 ± 0.11 (17)	7.70 ± 0.11 (36)	7.32 ± 0.09 (101)	7.45 ± 0.14 (20)	7.54 ± 0.09 (36)
Co	–	–	–	–	5.88 ± 0.14 (2)	–	–
Ni	–	6.36 ± 0.07 (4)	6.11 ± 0.11 (6)	6.35 ± 0.23 (11)	6.19 ± 0.18 (41)	6.27 ± 0.13 (6)	6.41 ± 0.16 (13)
Cu	–	–	–	–	4.41 ± 0.14 (1)	–	–
Zn	–	–	–	–	4.78 ± 0.14 (2)	–	–
Ga	–	–	–	–	–	–	–
Sr	–	2.55 ± 0.12 (1)	1.67 ± 0.12 (1)	2.96 ± 0.14 (2)	3.23 ± 0.14 (1)	1.36 ± 0.18 (1)	–
Y	–	3.14 ± 0.12 (1)	2.24 ± 0.12 (1)	2.82 ± 0.14 (1)	2.51 ± 0.17 (10)	3.03 ± 0.29 (3)	2.85 ± 0.17 (1)
Zr	–	–	–	–	3.18 ± 0.20 (10)	2.98 ± 0.18 (1)	–
Ba	–	3.78 ± 0.12 (2)	3.11 ± 0.12 (1)	2.48 ± 0.20 (3)	2.75 ± 0.13 (3)	2.69 ± 0.18 (2)	2.43 ± 0.17 (2)
La	–	–	–	–	1.60 ± 0.14 (2)	–	–
Ce	–	–	–	–	1.69 ± 0.14 (2)	–	–
Pr	–	–	–	–	–	–	–
Nd	–	–	–	–	1.72 ± 0.20 (5)	–	–

The difficulty increases for heavily blended spectra of stars with $v \sin i$ much higher than this value, even for high-resolution and high S/N data.

All the above-mentioned factors influenced our derived atmospheric parameters and chemical abundances. The chemical abundances are also affected by inaccurate atmospheric parameters. The influence of errors in atmospheric parameters on the derived chemical abundances can be checked by perturbing the synthetic spectrum by the adopted step size in the grid of atmospheric models. For example, $\Delta T_{\rm eff} = 100$ K leads to changes in abundances smaller than 0.1 dex in most cases. Similarly, $\Delta \log g = 0.1$ changes chemical abundance by about 0.05 dex, and $\Delta \xi_{\rm t} = 0.1$ km s^{-1} changes abundances by 0.15 dex at most. It should be noted here that the uncertainty on the microturbulence velocity increases with $v \sin i$, from 0.1 km s^{-1} for small and moderate velocities, to 0.4 km s^{-1} for rapid rotators. Chemical abundances determined for rapidly rotating stars are affected by the greatest uncertainty. The combined errors of chemical abundances were calculated as:

$$\Delta \log \epsilon_{el}^{\rm tot} = \sqrt{\left(\Delta \log \epsilon_{el}^{T_{\rm eff}}\right)^2 + \left(\Delta \log \epsilon_{el}^{\log g}\right)^2 + \left(\Delta \log \epsilon_{el}^{\xi_{\rm t}}\right)^2}$$

In most cases $\Delta \log \epsilon_{el}^{\rm tot}$ was less than 0.20 dex.

4.4 Comparison of results from different methods

4.4.1 Interstellar reddening

The $E(B-V)$ values from the KIC, $E(B-V)$(KIC), and those determined here from the equivalent widths of sodium D_2 lines, $E(B-V)$(Na), are given in Table 3. The distributions of these parameters are presented in Fig. 1. It is clear that the photometric interstellar reddening given in the KIC is higher than $E(B-V)$(Na). The average value of $E(B-V)$(KIC) is equal to 0.09 mag, whereas from sodium lines it is 0.03 mag. The reddenings obtained from Na D_2 lines are lower than 0.10 mag for all stars, except for KIC 9552758 (HD 190293) and KIC 8915335 (HD 190566), for which they equal 0.14 mag. We can see from Fig. 2 that the differences between interstellar reddenings obtained from Na D_2 lines and those listed in KIC slightly increase with effective temperature. As explained by Brown et al. (2011), the values of $E(B-V)$ given in the KIC were approximated using a simple model of dust distribution and with an adopted disk scale-height of 150 pc – larger than suggested by earlier estimates (e.g. Koppen & Vergely 1998; Marshall et al. 2006). Brown et al. (2011) assumed a wavelength dependence of reddening taken from Cardelli, Clayton & Mathis (1989) and used $R_{\rm V} = 3.1$ in all cases. As described by Brown et al. (2011), reddening was precomputed for all filters and for a range of stellar parameters. Then, the authors calculated the reddening vectors for typical stars

Downloaded from http://mnras.oxfordjournals.org/ at The Library on May 18, 2016

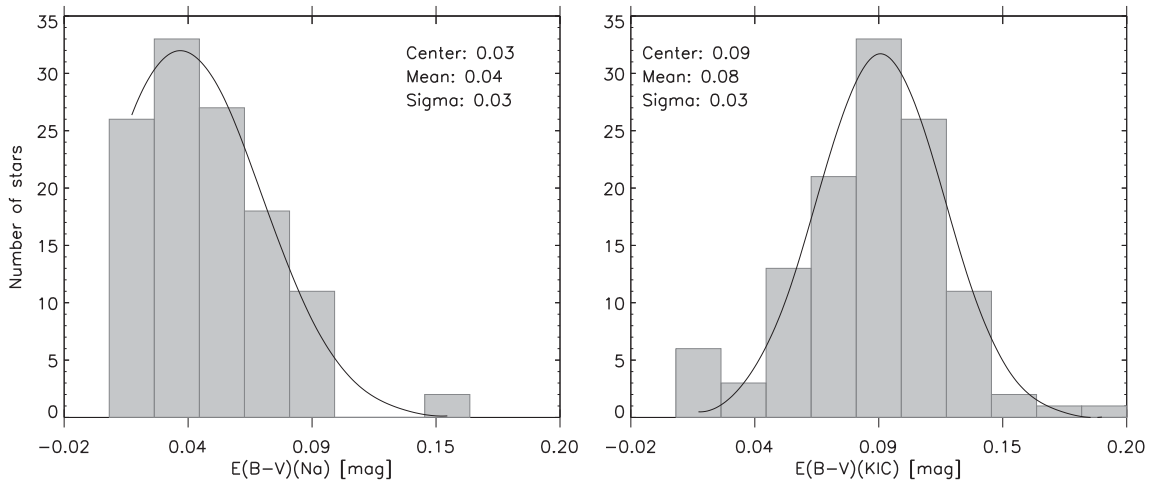

Figure 1. Distributions of $E(B-V)$(Na) (left-hand panel) and $E(B-V)$(KIC) (right-hand panel). Gaussian fits are shown by solid lines. Central values, arithmetic means and standard deviations of both distributions are indicated in figures.

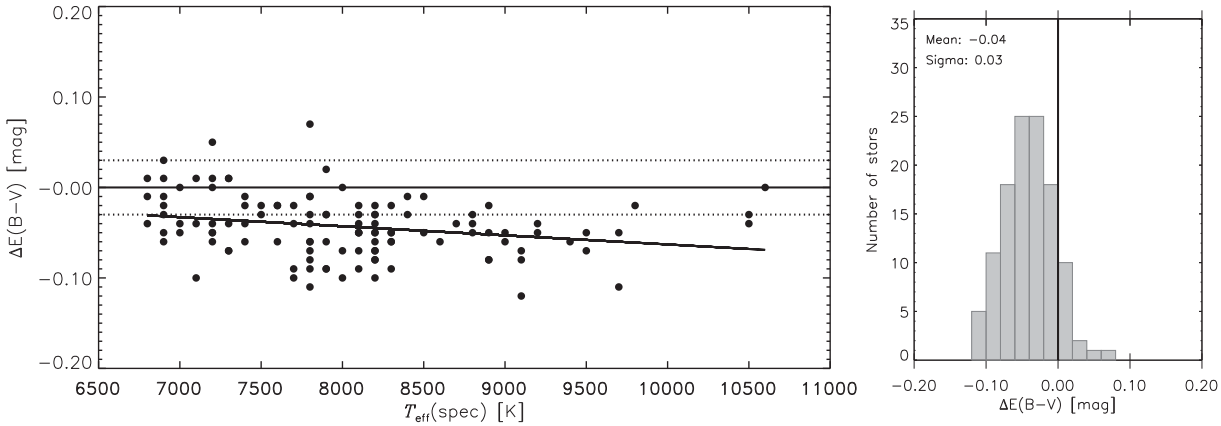

Figure 2. Left-hand panel: Differences $\Delta E(B-V) = E(B-V)$(Na) $- E(B-V)$(KIC) as a function of $T_{\rm eff}$(spec). A linear function is fitted. The dotted horizontal line indicates a difference of ± 0.03 mag. Right-hand panel: Distribution of differences $\Delta E(B-V)$. Arithmetic mean and standard deviation of the distribution are indicated in the figure.

in the *Kepler* field ($T_{\rm eff} = 5000$ K, $\log g = 4.0$ and [M/H] $= 0.0$) and applied them to all stars. Values of interstellar reddening influenced the other parameters determined from KIC photometry, especially the effective temperatures. For this reason, it is necessary to check the available KIC $E(B-V)$ values by determining them with an independent method.

4.4.2 *Effective temperatures*

The effective temperatures determined using the three methods described in Section 4 are presented in Table 3 and compared in Fig. 3, where the differences between $T_{\rm eff}$(spec) obtained from the analysis of the high-resolution spectra and values taken from the KIC, $T_{\rm eff}$(KIC), and from SED fitting, $T_{\rm eff}$(SED), are shown as a function of $T_{\rm eff}$(spec).

For most of the stars, the values of $T_{\rm eff}$(spec) $- T_{\rm eff}$(KIC) agree to within ± 300 K. Differences larger than 500 K occur for stars with peculiarities identified in their spectra (KIC 3231985, 4150611, and 8703413) and for some rapidly rotating stars with $v \sin i$ exceeding 100 km s^{-1} (KIC 11506607, 3347643, 4681323, 5471091, and 6450107). The Spearman's and Kendall's rank correlation coefficients between $T_{\rm eff}$(spec) $- T_{\rm eff}$(KIC) and $T_{\rm eff}$(spec) are equal to 0.25 and 0.17, respectively, indicating very low correlation. The $T_{\rm eff}$(KIC) values are underestimated for stars hotter than about 7500 K. For stars with lower effective temperatures, the agreement is better and the outliers can be explained by rapid rotation or chemical peculiarities in their spectra, which can influence the determination of atmospheric parameters. This result is in agreement with the previous spectroscopic determinations of atmospheric parameters given by Molenda-Żakowicz et al. (2011), Lehmann et al. (2011) and Tkachenko et al. (2013b), where the systematic underestimations of the KIC $T_{\rm eff}$ values for stars hotter than about 7000 K were pointed out. These deviations probably originate from incorrect values of interstellar reddening.

Recently, H2014 published a new catalogue of revised effective temperatures for 196 468 *Kepler* stars. The catalogue is based on a compilation of literature values for atmospheric properties ($T_{\rm eff}$, $\log g$ and [Fe/H]) derived from different methods, including photometry, spectroscopy, asteroseismology, and exoplanet transits. Effective temperature is available from the H2014 catalogue for all targets in our sample. In Fig. 3(a), we show the differences between $T_{\rm eff}$(H2014) and $T_{\rm eff}$(spec). As one can see, there is a similar scatter in differences [$T_{\rm eff}$(spec) $- T_{\rm eff}$(H2014)], as was the case for $T_{\rm eff}$(spec) $- T_{\rm eff}$(KIC). For stars with $T_{\rm eff} > 8000$ K, the differences [$T_{\rm eff}$(spec) $- T_{\rm eff}$(H2014)] are lower than for $T_{\rm eff}$(KIC), which means that the $T_{\rm eff}$(H2014) values are higher than $T_{\rm eff}$(KIC)

Downloaded from http://mnras.oxfordjournals.org/ at The Library on May 18, 2016

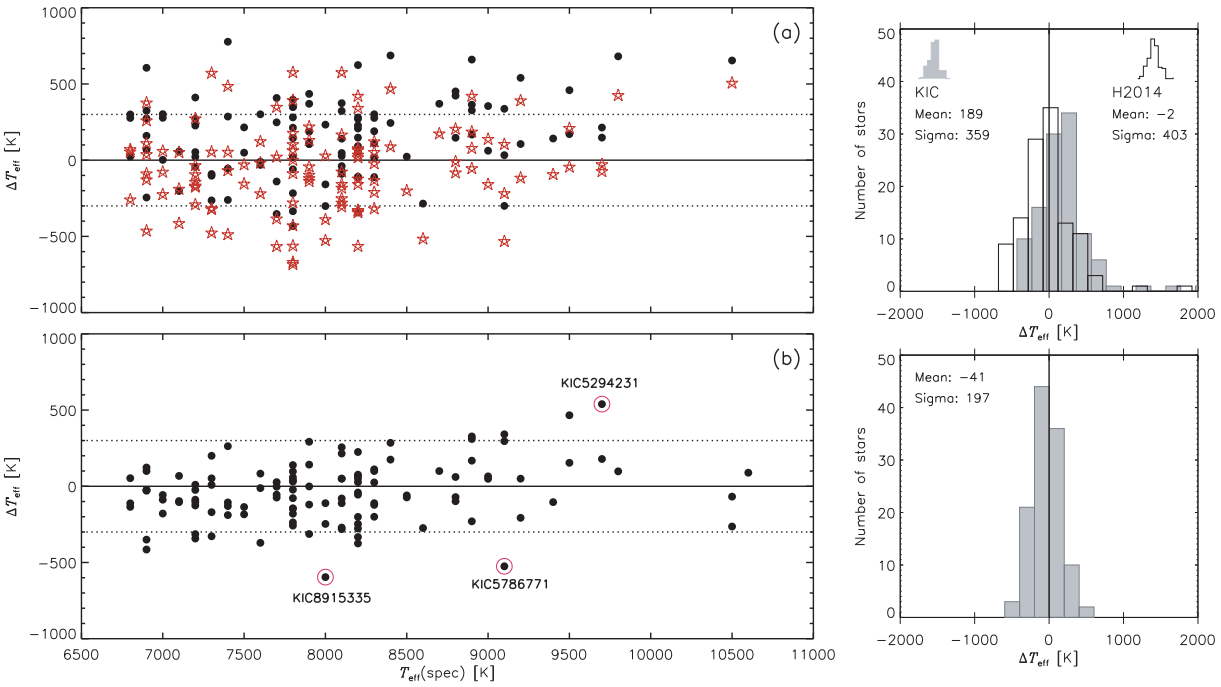

Figure 3. Comparison of effective temperatures derived by different methods. In panel (a), the differences $\Delta T_{\rm eff} = T_{\rm eff}({\rm spec}) - T_{\rm eff}({\rm KIC})$ are plotted as filled circles, whereas $\Delta T_{\rm eff} = T_{\rm eff}({\rm spec}) - T_{\rm eff}({\rm H2014})$ are shown as stars. In panel (b), $\Delta T_{\rm eff} = T_{\rm eff}({\rm spec}) - T_{\rm eff}({\rm SED})$ are plotted. The stars described in the text are indicated by names and open circles. The distributions of differences $\Delta T_{\rm eff}$ and their characteristics are given in the right-hand panels.

for such stars. Neither $T_{\rm eff}$(KIC) nor $T_{\rm eff}$(H2014) are systematically underestimated between 7000 and 8000 K.

Fig. 3(b) compares $T_{\rm eff}$(spec) with that determined from the spectral energy distribution, $T_{\rm eff}$(SED). The consistency between these two methods is good: there is no significant trend of $T_{\rm eff}({\rm spec}) - T_{\rm eff}({\rm SED})$ with effective temperature. The Spearman's and Kendall's rank correlation coefficients between $T_{\rm eff}({\rm spec}) - T_{\rm eff}({\rm SED})$ and $T_{\rm eff}$(spec) are equal to 0.23 and 0.16, respectively. This shows that the correlation is smaller than between $T_{\rm eff}({\rm spec}) - T_{\rm eff}({\rm KIC})$ and $T_{\rm eff}$(spec). The differences exceed 500 K only for three rapidly rotating stars: KIC 5294231, 5786771, and 8915335. The $T_{\rm eff}$(SED) analysis supports the claimed accuracy of our spectroscopic temperatures.

4.4.3 *Surface gravities*

Fig. 4 compares the $\log g$(spec) values obtained from high-resolution spectroscopy with those taken from the KIC, $\log g$(KIC), and the H2014 catalogue, $\log g$(H2014). For most stars the surface gravities are consistent to within ±0.2 dex. The distribution of differences $\log g({\rm spec}) - \log g({\rm KIC})$ and $\log g({\rm spec}) - \log g({\rm H2014})$ does not indicate any trend with surface gravity or effective temperature. The higher differences were determined mostly for rapidly rotating stars with $v \sin i > 100$ km s^{-1}. Irrespective of rotational velocity, spectroscopic surface gravity values determined from iron lines are adopted for subsequent analysis of these stars. The high-resolution spectra are much more sensitive to $\log g$ than the photometric indices upon which the KIC is based.

4.4.4 *Microturbulent velocities*

In Fig. 5, the derived values of microturbulence are shown as a function of effective temperature, with different symbols for CP and non-CP stars. The values of $\xi_{\rm t}$ obtained decrease towards higher effective temperature. For stars with $T_{\rm eff}$ between 7000 and 8000 K, $\xi_{\rm t}$ is within the range 2 to 4 km s^{-1}, for those with $T_{\rm eff}$ between 8000 and 9000 K, $\xi_{\rm t}$ is approximately 2 km s^{-1}, while for even higher values of $T_{\rm eff}$ microturbulence decreases to about 0.5 to 1 km s^{-1}. This behaviour is in agreement with the results of Gebran et al. (2014), based on the analysis of high-resolution spectroscopic data of 61 A field stars, and 55 A and 58 F stars in open clusters (Pleiades, Coma Berenices, Hyades and Ursa Major). The results are also in agreement with Smalley (2004). The determined microturbulent velocities of CP stars are similar to those of non-CP stars. According to Landstreet et al. (2009), the microturbulent velocity in Am stars is generally higher than in normal stars. This tendency is not seen in our sample. However, in Landstreet et al. (2009) it is not possible to directly compare the microturbulence velocities of the Am stars with normal stars of the same temperature, because, as Murphy (2014) notes, the temperature distributions do not overlap. We conclude that in our sample the distribution of microturbulent velocities among the Am stars appears to be the same as that of normal stars. As shown by Landstreet et al. (2009), the line profiles of slowly rotating Am stars show different asymmetries and anomalies caused by velocity fields. These asymmetries affect line shapes and equivalent widths and lead to higher microturbulence velocities in comparison with chemically normal A stars. However, since the analysis of Landstreet et al. (2009) is based on a sample of stars with low projected rotation velocity ($v \sin i < 12$ km s^{-1}), it cannot be ruled out that this phenomenon is diluted for faster rotators. It is beyond the scope of this paper to examine this effect in more detail.

As expected, the microturbulent velocity determined for the Ap star is small, $\xi_{\rm t} = 0.5 \pm 0.2$ km s^{-1} (e.g. Folsom et al. 2007).

4.4.5 *Iron abundances*

Fig. 6 compares the iron abundances derived from high-resolution spectra, $\log \epsilon$(Fe)(spec), with those from the KIC, $\log \epsilon$(Fe)(KIC).

Downloaded from http://mnras.oxfordjournals.org/ at The Library on May 18, 2016

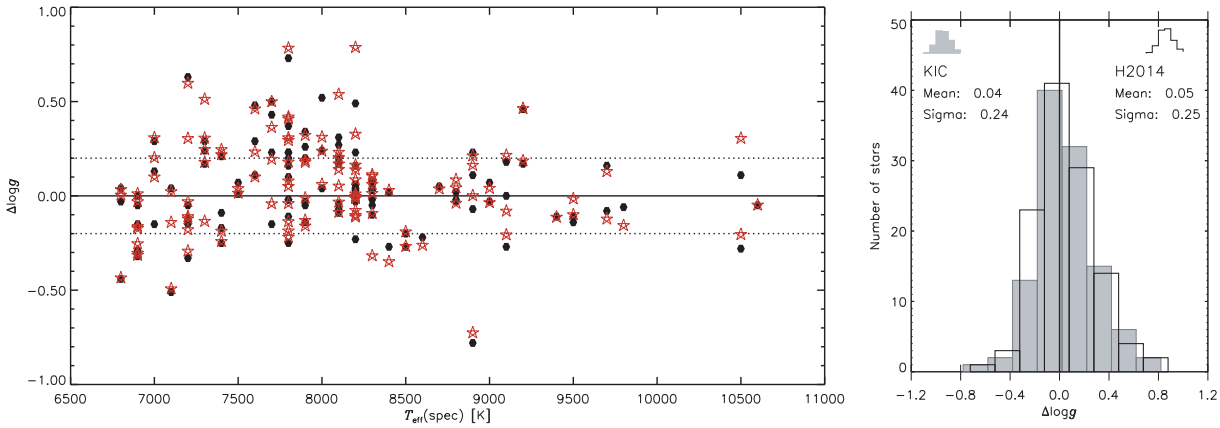

Figure 4. Left-hand panel: Differences $\Delta\log g = \log g(\mathrm{spec}) - \log g(\mathrm{KIC})$ (filled circles) and $\Delta\log g = \log g(\mathrm{spec}) - \log g(\mathrm{H2014})$ (stars) as a function of $T_{\rm eff}$(spec). Right-hand panel: Distributions of differences $\Delta\log g$ and their characteristics.

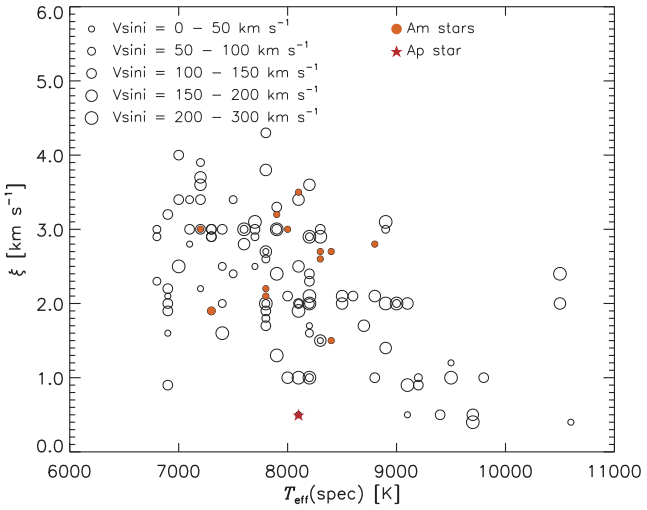

Figure 5. Microturbulent velocities as a function of effective temperature. Non-CP stars are shown as open circles, Am and Ap stars as filled circles and a star symbol, respectively. Sizes of symbols and Am depend on rotational velocity; see the legend.

As can be seen, the differences $\log\epsilon(\mathrm{Fe})(\mathrm{spec}) - \log\epsilon(\mathrm{Fe})(\mathrm{KIC})$ are strongly correlated with the iron abundance. The same situation occurs for differences between $\log\epsilon(\mathrm{Fe})(\mathrm{spec})$ and $\log\epsilon(\mathrm{Fe})$(H2014), taken from the H2014 catalogue. The Spearman's and Kendall's rank correlation coefficients are equal to 0.74 and 0.57, respectively. Only four stars (KIC 4150611, 6951642, 7119530, 7299869; the encircled symbols in Fig. 6) do not follow this general tendency.

KIC 4150611 is a possible triple system classified as F1V with weak metal lines suggesting spectral type A9. This classification was not confirmed by detailed analysis of chemical abundances, as iron abundance is only 0.16 dex lower than the solar abundance from Asplund et al. (2009). The other elements do not show significant deviations from the solar values either. This effect can be caused by analysing a triple object as a single one. Additionally, the rotational velocity of this star is 128 ± 5 km s^{-1}. For a star with $T_{\rm eff}$ =7400 K, this causes strong blending of all metal lines. It is worth mentioning that the differences between effective temperatures derived from the KIC photometry, SED, and high-resolution spectrum are also high for this star.

Rapid rotation ($v\sin i$ >120 km s^{-1}) is also likely to be responsible for the deviations in chemical abundances for the other three stars. Additionally, the analysis of high-resolution spectra resulted in higher iron abundances for KIC 4768731, an Ap (SrCrEu) star for which a high iron abundance is expected. The same trend of $\log\epsilon(\mathrm{Fe})(\mathrm{spec}) - \log\epsilon(\mathrm{Fe})(\mathrm{KIC})$ with iron abundance was noticed by Tkachenko et al. (2013b). We found no correlation of $\log\epsilon(\mathrm{Fe})(\mathrm{spec}) - \log\epsilon(\mathrm{Fe})(\mathrm{KIC})$ differences with effective temperature or surface gravity.

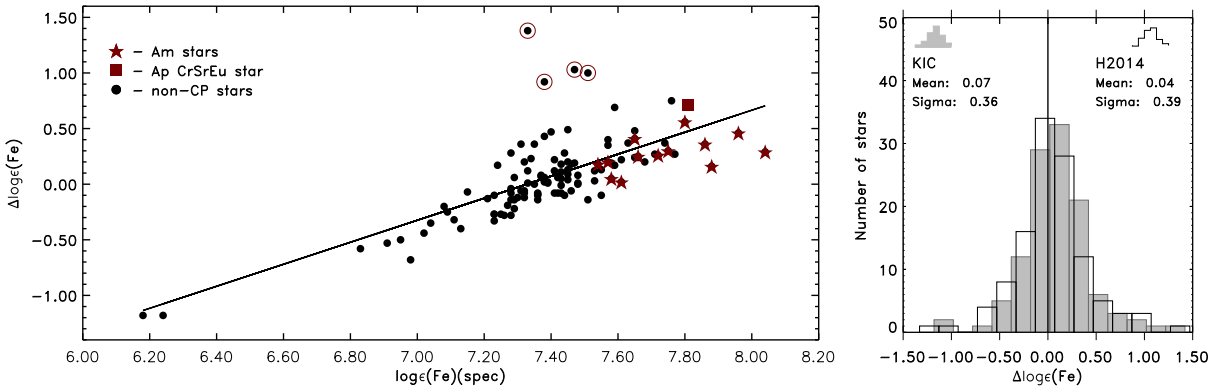

Figure 6. Left-hand panel: Differences $\Delta\log\epsilon(\mathrm{Fe}) = \log\epsilon(\mathrm{Fe})(\mathrm{spec}) - \log\epsilon(\mathrm{Fe})(\mathrm{KIC})$ as a function of $\log\epsilon(\mathrm{Fe})(\mathrm{spec})$. Non-CP and CP stars are plotted by different symbols as explained in the legend. The four most deviant objects are encircled (see the description in the text). The line is the linear fit to all points. Right-hand panel: Distribution of differences $\Delta\log\epsilon(\mathrm{Fe})$ and their characteristics.

Downloaded from http://mnras.oxfordjournals.org/ at The Library on May 18, 2016

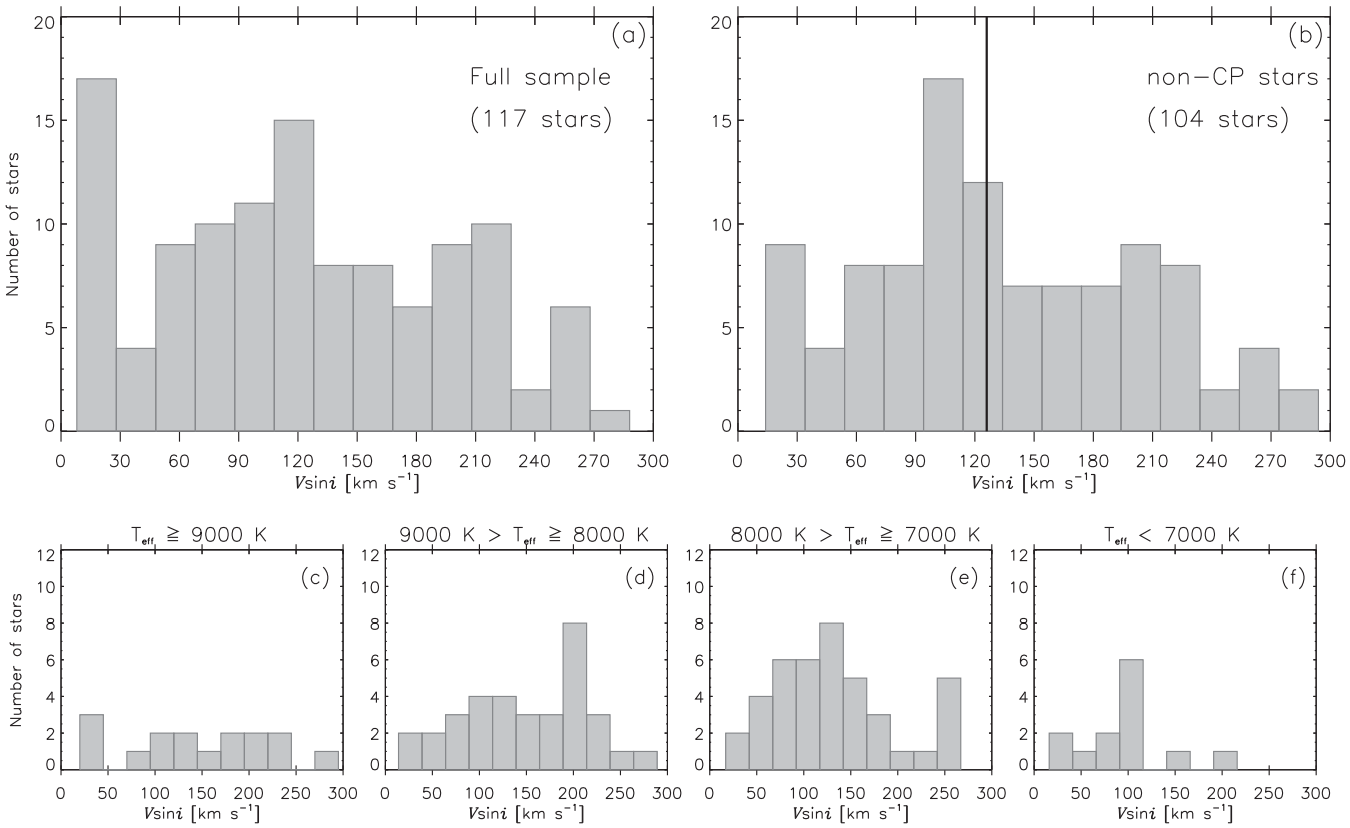

Figure 7. Distribution of rotational velocities for all analysed stars (a) and for all non-CP stars (b). Panels (c), (d), (e) and (f) show distributions of $v \sin i$ for stars with $T_{\rm eff} \geq 9000$ K, $9000 > T_{\rm eff} \geq 8000$ K, $8000 > T_{\rm eff} \geq 7000$ K, and $T_{\rm eff} < 7000$ K, respectively.

5 PROJECTED ROTATIONAL VELOCITIES

Rotational velocity is one of the fundamental parameters that influences stellar evolution. It has been frequently demonstrated that stellar rotation strongly depends on spectral type, with most A stars being rapid rotators (e.g. Royer 2009; Abt 2009).

Fig. 7(a) shows the distribution of derived values of $v \sin i$. The stars analysed have projected rotational velocities ranging from 8 to about 280 km s^{-1}. Stars with $v \sin i$ lower than 40 km s^{-1} are considered here as slowly rotating stars. There are 21 such objects in our sample. The obvious members of this group are all either Am or Ap (CrSrEu) stars. These objects will be thoroughly discussed in the next section. Another slowly rotating star, KIC 3231985, also shows small peculiarities in its spectrum and was classified as A4 IV Ca weak (A3). Fig. 7(b) shows the distribution of $v \sin i$ for all non-CP stars. One can see that the peak for slow rotation has disappeared and the mean value of $v \sin i$ for this sample is equal to 134 km s^{-1}. The maximum of the distribution is located around 110 km s^{-1}. This result is consistent with the rotational velocities of A stars given in the literature (Royer 2009). Abt (2000) pointed out that most of the normal A0–F0 main-sequence stars have equatorial rotational velocities greater than 120 km s^{-1}. Panels (c)–(f) in Fig. 7 show distributions of $v \sin i$ for stars with different ranges of $T_{\rm eff}$. Most of the stars with $T_{\rm eff} < 7000$ K have projected rotational velocities below 100 km s^{-1}, consistent with the predictions for the late A and early F stars (Royer 2009).

There are nine slowly rotating stars in our sample that were not classified as CP objects. Three of them were classified as F stars: KIC 6519869 (F1 IV-Vs), KIC 7661054 (F2.5 V), and KIC 4077032 (F2 IIIs). On average, F stars have smaller rotation velocities than A stars. The rotation velocity drops rapidly from high values (>100 km s^{-1}) for late A stars to low values (<20 km s^{-1}) for late F stars (Noci, Pomilia & Ortolani 1986; Royer 2009). All slowly rotating non-CP F stars have abundance patterns close to solar, except for some elements. For KIC 4077032, heavy and rare-earth elements are overabundant, while for KIC 6519869 only abundances of elements derived from weak blends are significantly different from solar. Four of the slow rotators were classified as mid-A stars: KIC 10721930 (A5 IV), KIC 3231985 (A4 IV Ca weak (A3)), KIC 5355850 (A5 IVs), and KIC 8386982 (A4 IV/V:). For KIC 10721930, heavy and rare-earth elements are overabundant. For KIC 3231985, almost all elements are overabundant. This star has been identified as a binary (e.g. Dommanget & Nys 2002; Fabricius et al. 2002). Two objects were classified as early-A stars: KIC 12153021 (A2 IV-V) and KIC 12736056 (A0.5 IIIs).

The occurrence of non-CP A stars with low $v \sin i$ has been discussed in many papers (e.g. Takeda et al. 2008; Abt 2009; Royer et al. 2014). Abt (2009) presented this problem in detail, considering binarity and the amount of time necessary for slow rotators to become Ap or Am stars by a diffusion mechanism (see also Talon, Richard & Michaud 2006; Michaud & Richer 2013). The frequency of binaries among A stars turned out to be normal. On the other hand, the time-scale for developing peculiarities is rapid for Ap(Si), Ap(HgMn), and Am stars, but slow for Ap(SrCrEu) stars, for which it takes about half of their main-sequence lifetime. According to Abt (2009), if a constant formation rate of field A stars is assumed, about half of the potential Ap(SrCrEu) stars will appear as normal slow rotators and that is why there are normal slow rotators in the A0–A3 group. Therefore, slowly rotating, non-CP

Downloaded from http://mnras.oxfordjournals.org/ at The Library on May 18, 2016

stars could be Ap stars that already underwent magnetic braking, but do not yet show chemical peculiarity. Accordingly, the five slowly rotating stars from our sample (KIC 10721930, 12153021, 12736056, 5355850, and 8386982) might become Ap(CrSrEu) stars in the future.

A more probable reason for the low observed $v \sin i$ in some A stars is the projection effect. The influence of this effect on the spectral lines of Vega has been investigated by Gulliver, Hill & Adelman (1994). For many years Vega was considered as a standard star with $v \sin i$ equal to 24 km s^{-1} (e.g. Royer, Zorec & Gómez 2007). Gray (1985) first suggested that Vega is a rapid rotator seen pole-on. Gulliver et al. (1994) analysed high-resolution, high S/N spectra of Vega and found two distinct types of profiles. The strong lines exhibit classical rotational profiles with enhanced wings, but the weak lines have different, flat-bottomed profiles. Gulliver et al. (1994) used ATLAS9 model atmospheres and SYNTHE synthetic spectra to model the spectral lines and confirmed that Vega is in fact a rapidly rotating, nearly pole-on star with a gradient in temperature and gravity in the photosphere. The equatorial rotational velocity of Vega ($V_{\rm eq} = 245 \pm 15$ km s^{-1}) and inclination ($5\overset{\circ}{.}1 \pm 0.3$) were derived by fitting the flat-bottomed line profiles of Fe I 4528 Å and Ti II 4529 Å. To investigate the effect that low inclination has on the observed spectrum of a rapid rotator, high-resolution ($R \geq 70\,000$), and very high S/N ~1000 spectra are necessary. Takeda et al. (2008) found that lines of ionized elements in the spectrum of Vega show classical profiles, while the lines of neutral elements display very characteristic shapes: from flat-bottomed to reversed profiles, due to the temperature gradient from the pole to the equator.

Royer et al. (2012) analysed a sample of A stars to find possible rapid rotators seen pole-on. The line profiles in each spectrum were analysed globally, using a least-square deconvolution (LSD) method (Donati et al. 1997; Kochukhov, Makaganiuk & Piskunov 2010) to enhance the signal and recover the broadening function. To investigate the possibility that the slow rotators in our sample are in fact rapid rotators seen pole-on, we followed the methods presented by Gulliver et al. (1994) and Takeda et al. (2008). We used the revised LSD code (Tkachenko et al. 2013a) to calculate the LSD profiles for intrinsic line depths from 0 to 0.6 and from 0.6 to 1.0, which enables the distinction between the line profiles of strong and faint lines in the spectra of the slow rotators. All line lists were computed with the individual parameters of $T_{\rm eff}$, $\log g$, $v \sin i$, $\xi_{\rm t}$ and [M/H] determined in this paper. The boundary for the separation of line depths was chosen so that the S/N in both LSD profiles, computed from weak and strong lines, were approximately equal. The wavelength range used (4890 to 5670 Å) included the region between Hβ and the first strong telluric lines. We found no significant difference in profile shapes for any of the investigated stars, which can be attributed to the insufficient quality of our spectra.

6 CHEMICAL ABUNDANCES

In Table 5 the average abundances for the stars in our sample are compared with the photospheric solar values of Asplund et al. (2009). Only the abundances of Mg, Ti, and Fe were derived for all stars. We excluded the O I 7771-5 Å triplet from our analysis and used other O I lines (e.g., 5331, 6157, 6158, and 6456 Å) that are much less affected by non-LTE effects (e.g. Przybilla et al. 2000). Lines of heavy elements except for Sr, Y, Ba, and rare-earth elements are very sparse in spectra of A stars. Abundances of these elements were investigated only for slowly and moderately rotating stars and in most cases, only one or two blends were available.

Table 5. Average abundances for the entire sample and the non-CP stars compared to the solar values of Asplund et al. (2009).

El.	No. of all stars	Normal stars $\log \epsilon$(El)	All stars $\log \epsilon$(El)	Solar values
C	116	8.47 ± 0.23	8.42 ± 0.27	8.43
N	29	8.08 ± 0.45	8.01 ± 0.42	7.83
O	91	8.88 ± 0.28	8.82 ± 0.31	8.69
Na	76	6.52 ± 0.49	6.54 ± 0.46	6.24
Mg	117	7.61 ± 0.28	7.61 ± 0.27	7.60
Al	20	6.31 ± 0.33	6.47 ± 0.32	6.45
Si	115	7.53 ± 0.24	7.55 ± 0.24	7.51
P	1	5.32	5.32	5.41
S	40	7.37 ± 0.21	7.37 ± 0.20	7.12
K	4	5.52 ± 0.14	5.58 ± 0.17	5.03
Ca	116	6.43 ± 0.31	6.38 ± 0.34	6.34
Sc	115	3.14 ± 0.42	3.04 ± 0.50	3.15
Ti	117	4.98 ± 0.26	4.98 ± 0.25	4.95
V	61	4.21 ± 0.51	4.29 ± 0.51	3.93
Cr	116	5.58 ± 0.20	5.65 ± 0.28	5.64
Mn	92	5.43 ± 0.35	5.45 ± 0.33	5.43
Fe	117	7.36 ± 0.24	7.40 ± 0.26	7.50
Co	18	5.18 ± 0.59	5.36 ± 0.55	4.99
Ni	115	6.25 ± 0.27	6.31 ± 0.30	6.22
Cu	27	4.01 ± 0.43	4.26 ± 0.53	4.19
Zn	39	4.45 ± 0.39	4.67 ± 0.49	4.56
Ga	5	3.22 ± 0.03	3.35 ± 0.14	3.04
Sr	70	2.79 ± 0.75	2.98 ± 0.84	2.87
Y	93	2.38 ± 0.44	2.48 ± 0.50	2.21
Zr	58	3.10 ± 0.36	3.12 ± 0.38	2.58
Ba	108	2.64 ± 0.52	2.80 ± 0.70	2.18
La	24	1.35 ± 0.58	1.84 ± 0.93	1.10
Ce	17	2.12 ± 0.44	2.46 ± 0.40	1.58
Pr	4	1.12 ± 0.65	1.14 ± 0.53	0.72
Nd	15	1.85 ± 0.23	2.13 ± 0.35	1.42
Sm	2	1.58	2.11 ± 0.74	0.96
Eu	10	0.46 ± 0.21	1.34 ± 0.81	0.52
Gd	3	1.78 ± 0.08	1.94 ± 0.30	1.07
Dy	4	1.92 ± 0.20	1.92 ± 0.16	1.10
Er	1	1.48	1.48	0.92

In Fig. 8, the determined average abundances for all stars are compared with the solar abundances of Asplund et al. (2009). In Fig. 9, histograms show the distribution of abundances of the iron-peak elements, Ti, Cr, Mn, Fe, Sc, and Ca. The average abundances of most of the light and iron-peak elements are close to the solar values. The largest differences occur for the elements represented by weak blends only. Naturally, the abundances of some elements determined for CP stars are significantly different from the solar values. For instance, the highest Cr abundance, $\log \epsilon$(Cr) = 7.17 ± 0.26, was determined for the Ap CrSrEu star KIC 4768731, and the lowest abundances of Sc were derived for Am stars.

We found that apart from 14 CP stars, there are two low-metallicity objects in our sample, KIC 9828226 and KIC 8351193. KIC 9828226 was classified as an A1.5 V star for which the metal line spectrum is weak and matches A0 type. The moderate rotational velocity, 88 ± 9 km s^{-1}, allowed us to obtain the abundances of Mg, Si, Ca, Sc, Ti, Cr, Fe, Ni, Sr, C, and N. All these elements are underabundant. KIC 8351193 (HD 177152) was classified as a B9.5: star. With a rotational velocity of 162 km s^{-1}, the spectrum of this star is almost featureless. It was possible to determine only the abundances of Mg, Ti, and Fe on the basis of single lines. All

Downloaded from http://mnras.oxfordjournals.org/ at The Library on May 18, 2016

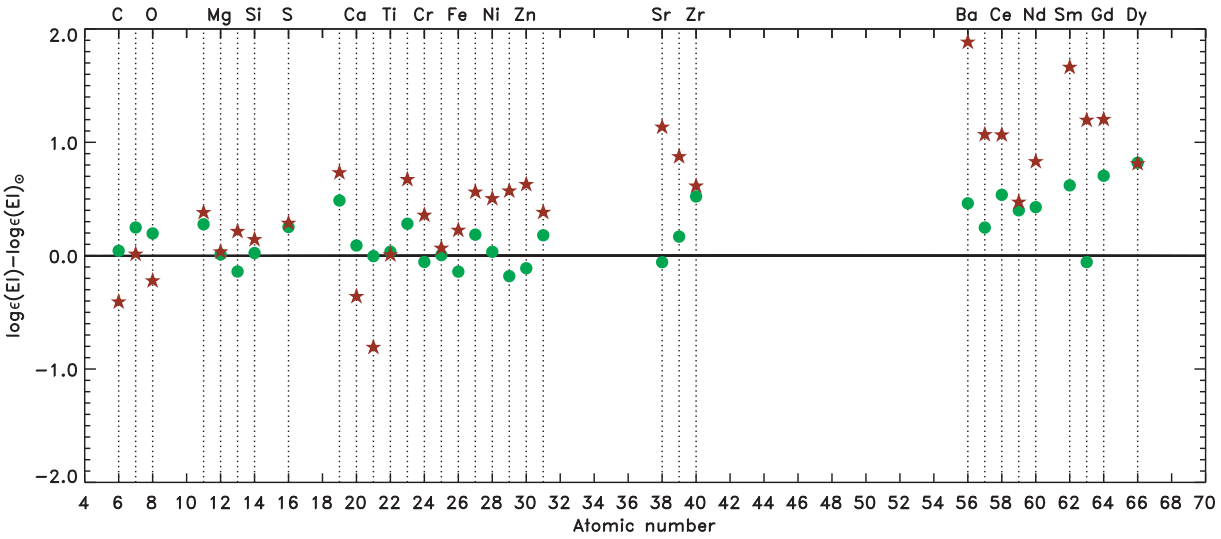

Figure 8. Difference between the obtained chemical abundances and solar values (Asplund et al. 2009) as a function of atomic number. The results for non-CP stars are given as filled circles and for CP stars as filled stars.

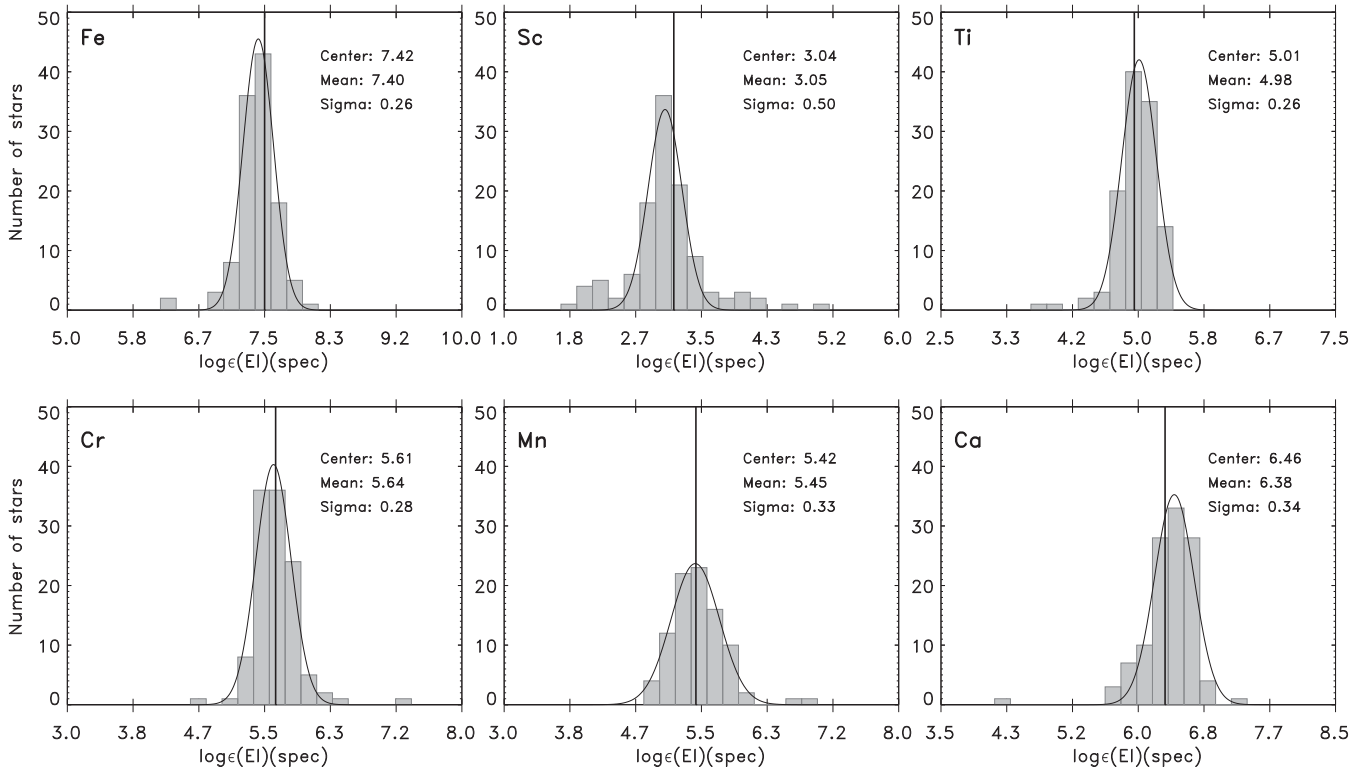

Figure 9. Distributions of the abundances of the elements: Fe, Sc, Ti, Cr, Mn, and Ca in the analysed sample of stars. The solar abundances taken from Asplund et al. (2009) are shown as vertical lines.

these elements are underabundant. However, because of the high $v \sin i$, a small error in continuum location significantly changes the results. Tkachenko et al. (2013b) analysed the high-resolution TLS spectrum of this star and obtained $T_{\rm eff} = 9980 \pm 250$ K and $\log g = 3.80 \pm 0.15$ dex from the analysis of Balmer lines. The effective temperature and surface gravity obtained in the present paper, $T_{\rm eff}$(spec) $= 10500 \pm 250$ K and $\log g$(spec) $= 4.1 \pm 0.1$ are higher than given by Tkachenko et al. (2013b). The high rotational velocities obtained in both papers are consistent within the error bars. Although Tkachenko et al. (2013b) also found a low metallicity for this star, their iron abundance of 5.15 dex is much lower than the value obtained in this paper (6.24 dex). The difference is caused mostly by differences in effective temperatures. The effective temperatures $T_{\rm eff}$(SED) and $T_{\rm eff}$(spec) of KIC 8351193 obtained in this paper are consistent with each other and with the values 10 210 K and 11 000 ± 400 K, determined from the SED and Strömgren photometry by Balona et al. (2011). On the basis of *Kepler* data, Balona et al. (2011) classified KIC 8351193 as a 'rotationally modulated' star with period of 0.567 67 d. We confirm this classification (see Section 7).

Downloaded from http://mnras.oxfordjournals.org/ at The Library on May 18, 2016

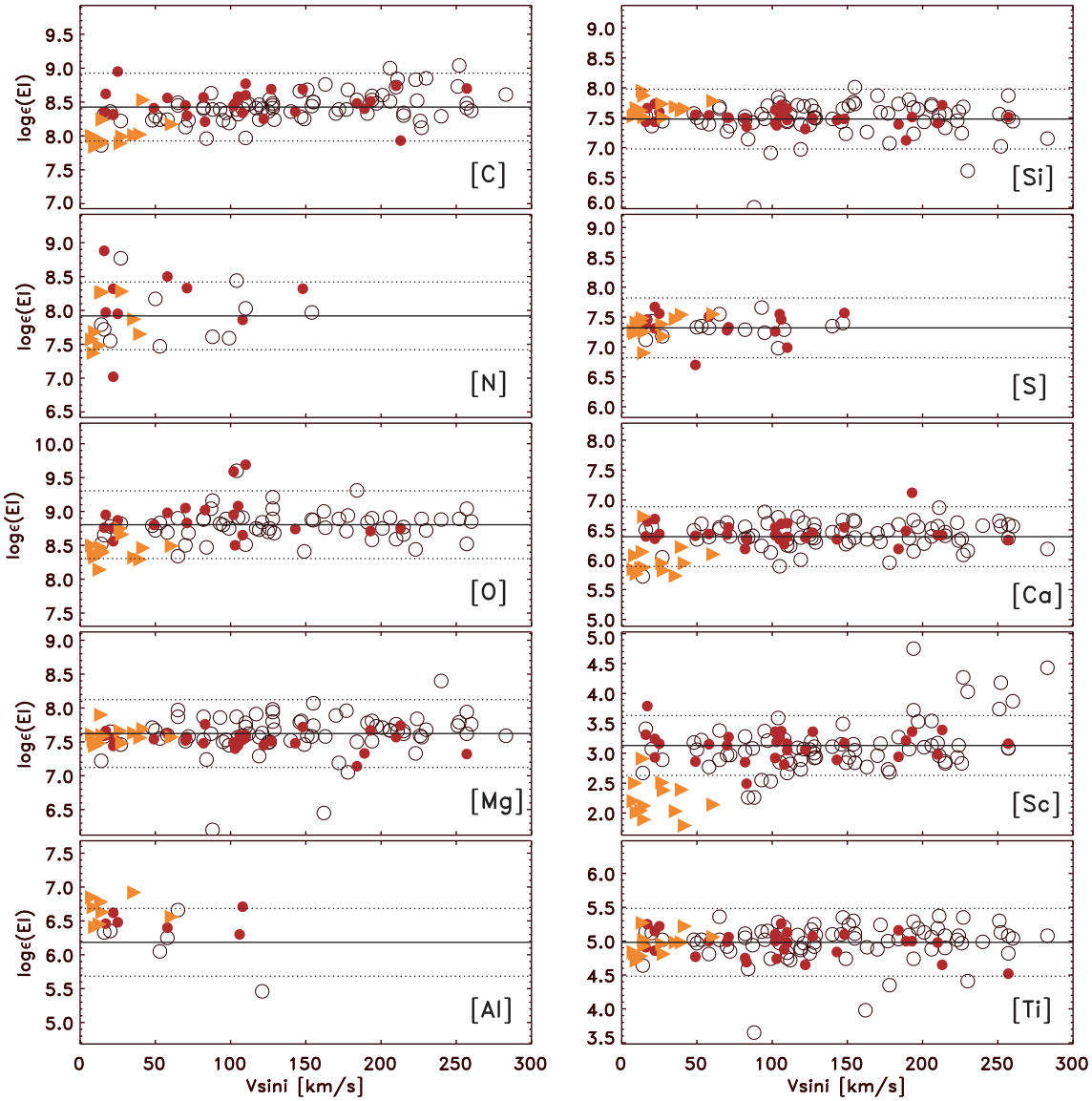

Figure 10. Abundances of different elements as a function of rotational velocity for CP stars (triangles), non-CP stars with $T_{\rm eff} > 7200$ K (filled circles), and non-CP stars with $T_{\rm eff} < 7200$ K (open circles).

6.1 Correlation of chemical abundances with other parameters

The analysis of a large sample of stars allowed us to search for correlations between the abundances of chemical elements and stellar parameters. We analysed separately three groups: the CP stars formed one group, and the normal stars were separated into hotter ($T_{\rm eff} > 7200$ K) and cooler ($T_{\rm eff} < 7200$ K) populations. For some elements, large scatter or a small number of stars with determined abundances prevents the correlation analysis. This is the case for most of the heavy and rare-earth elements. Comparing samples with hotter and cooler stars, we found a larger scatter of abundances for hotter stars, especially for $v \sin i$ higher than 150 km s^{-1}. The same effect was observed for the abundances of A and F stars in the Hyades (Gebran et al. 2010), Pleiades (Gebran & Monier 2008) and Coma Berenices open clusters (Gebran, Monier & Richard 2008).

No significant correlations of element abundances with effective temperature and surface gravity were found in the normal stars, with absolute values of Spearman's and Kendall's correlation coefficients less than ∼0.20. No significant correlations between the abundances of most elements and rotational velocity were found either. Typical relations for some elements are presented in Fig. 10. A small positive correlation was found between the abundances of C and $v \sin i$ for hotter stars, with correlation coefficients of about 0.3–0.4 according to both considered statistics. In an investigation of 23 normal A and F stars, Fossati et al. (2008) found no correlation between abundances and rotational velocity. A larger sample was examined by Takeda et al. (2008), who found negative correlations for C, O, Ca and strong positive correlations for the Fe-peak elements plus Y and Ba, with rotational velocity.

Significant positive correlations with iron abundance in normal stars were found for almost all elements (see Fig. 11). The highest correlation coefficients were obtained for light elements Na, Mg and Si, iron-peak elements Ca, Ti, Cr, Mn, Ni, and heavy elements Sr and Ba, all of which have correlation coefficients larger than 0.50. Less significant positive correlations were obtained for Sr and Y, for which both correlation coefficients were smaller than 0.40.

Downloaded from http://mnras.oxfordjournals.org/ at The Library on May 18, 2016

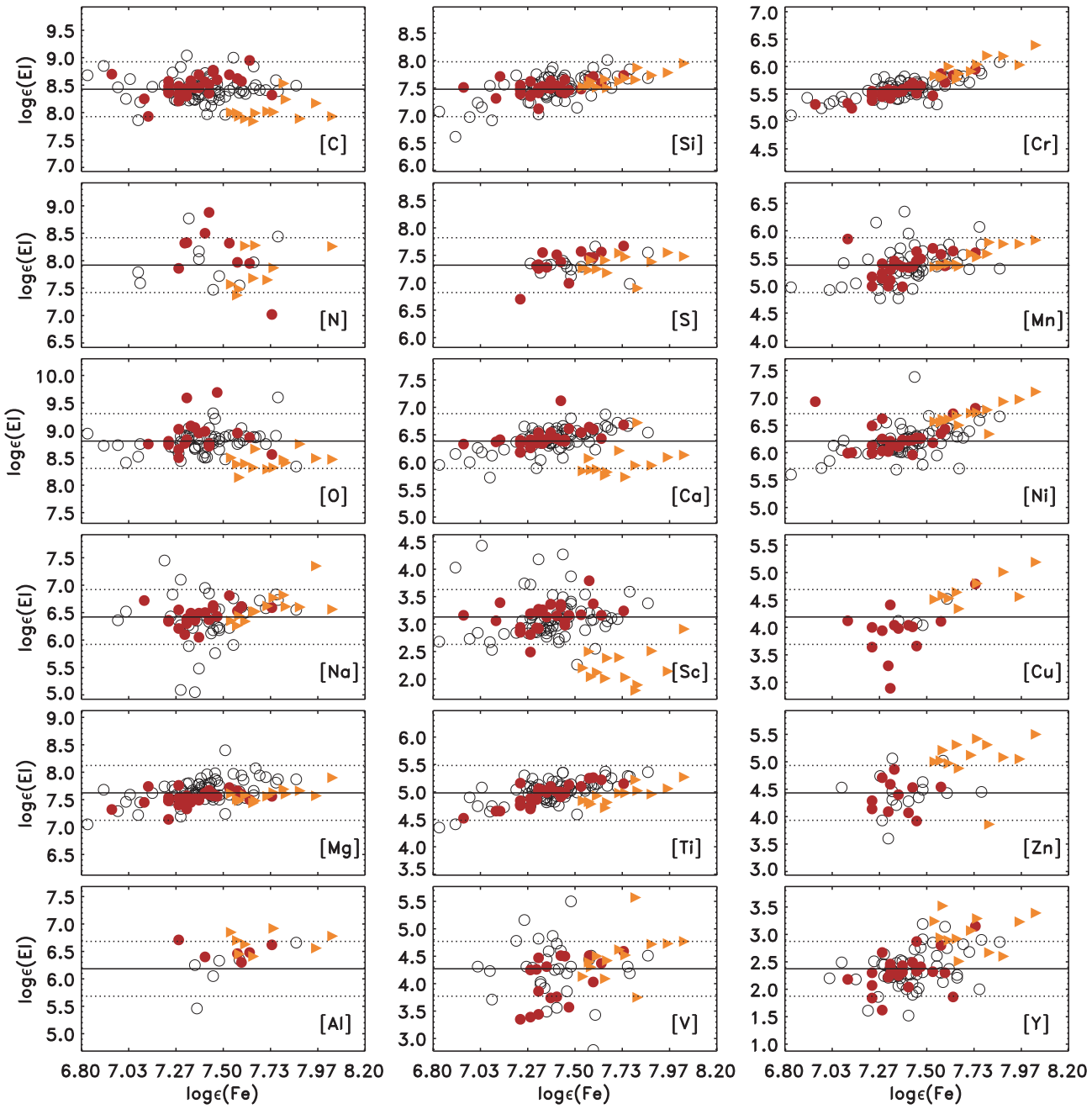

Figure 11. Abundances of different elements as a function of iron abundance for CP stars (triangles), non-CP stars with $T_{\rm eff} > 7200$ K (filled circles), and non-CP stars with $T_{\rm eff} < 7200$ K (open circles).

Takeda et al. (2008) also found strong positive correlations between the abundances of Si, Ti and Ba, and that of Fe.

We classified 21 CP stars in our sample, including 17 Am stars, one Ap CrSrEu, two λ Boo stars and one He-strong B star. We checked for correlations between abundances in Am stars and their atmospheric parameters, iron abundances, and rotational velocities. The abundances of most chemical elements appeared to be independent of the effective temperature. The negative correlation determined for O and the positive correlations found for Cu, Zn, and Zr could be caused by the small sample size. We found no correlations between abundances and surface gravity. On the other hand, the abundances of Na, Si, Ti, V, Cr, Mn, Ni, Cu, and rare-earth element La were all positively correlated with the iron abundance (Fig. 11). The only element found to be negatively correlated with iron was Zr, with a correlation coefficient of −0.20, according to Spearman's statistic. The abundances of many elements were also found to be strongly correlated with that of iron for non-CP stars.

The correlation between Na and Fe abundances was discussed by Takeda et al. (2012), who performed a non-LTE analysis of the abundances of alkali elements (Li, Na, and K) determined from the Li I 6708 Å, Na I 5682/5688 Å, and K I 7699 Å lines for 24 slowly rotating A stars ($v \sin i < 50$ km s^{-1}) in the broad temperature range 7000 K $< T_{\rm eff} <$ 10000 K. Many of these stars showed Am peculiarities to different degrees. They found a significant trend of Na abundances with Fe, independent of $T_{\rm eff}$. This means that Na becomes enriched along with Fe in accordance with the degree of

Downloaded from http://mnras.oxfordjournals.org/ at The Library on May 18, 2016

Am peculiarity. The same trend was derived for our sample of stars with a Spearman's correlation coefficient of +0.76. The positive correlation of Na abundance with Fe disagrees with the predictions of atomic diffusion theory (e.g. Talon et al. 2006). The same is true of Si abundances in Am stars, where we see a positive correlation of +0.80, according to Spearman's statistic, that is not theoretically expected.

No significant correlations with $v \sin i$ were found for the abundances of any element, albeit in a small analysed range of $v \sin i$. This contradicts the finding of Fossati et al. (2008) who analysed Am stars in the Praesepe cluster and reported strong correlations between abundances and $v \sin i$ of Am stars for all peculiar elements, except for Sc and Ti. One reason for the contradiction may be that the field stars analysed here have different ages and initial chemical composition.

6.2 CP stars

There are two main classes of CP stars among the main-sequence population I stars: the metallic line (Am) and the peculiar A stars (Ap). The Am stars manifest overabundances of most iron-peak elements and some heavy elements like Zn, Sr, Zr and Ba, and underabundances of Ca and Sc (Gray & Corbally 2009). These anomalies are explained by radiative diffusion in a non-magnetic star (e.g. Richard 2005; Talon et al. 2006). Their projected rotational velocities are generally smaller than those of normal A stars (Abt & Hudson 1971), which permits the segregation of elements by diffusion (Abt & Moyd 1973). The majority of Am stars are members of close binary systems, where their slow rotation results from tidal braking.

The Ap stars form the second group of CP stars with overabundances of some elements, such as Si, Sr, Cr, and rare-earth elements (e.g. Kurtz et al. 2007a,b). Most of these stars have strong magnetic fields with polar field strengths typically of several kilogauss (Hubrig et al. 2005; Kurtz et al. 2006). These stars have much slower rotational velocities than normal A and B stars. The distribution of chemical abundances changes both horizontally, with the formation of spots, and vertically, where they are stratified (e.g. Ryabchikova, Leone & Kochukhov 2005; Ryabchikova 2014; Kochukhov et al. 2015). The abundance anomalies and spots are caused by diffusion in the presence of a magnetic field (e.g. Babel 1993; Turcotte 2003).

There are other classes of CP stars, such as the λ Boötis stars, which are a class of metal-weak population I A stars (Gray & Corbally 2009). They are characterized by a weak Mg II 4481 Å line and solar abundances of C, N, O, and S (Gray 2005). Their projected rotational velocity distribution matches that of normal A stars (Abt & Morrell 1995; Gray & Corbally 2009). The metal deficiencies of λ Boo can be distinguished from those of population II stars on the basis of detailed abundance analyses (Paunzen et al. 2014). This suggests that the abundances of λ Boo stars are restricted to the outer layers of their atmospheres and can be explained by accretion of dust-depleted circumstellar material (Venn & Lambert 1990; King 1994).

There are 20 peculiar A stars in our sample (see Table 6 and Fig. 12), which comprises 17 Am stars, one Ap star (KIC 4768731), and two λ Boötis candidates (KIC 9828226 and KIC 5724440).

Four of the Am stars were previously known from multicolour photometry (Mendoza 1974) and spectroscopy (Floquet 1975). These are KIC 8323104, 8703413, 9117875, and 9204718. KIC 8323104 has a very low $v \sin i$ of 10 ± 1 km s^{-1}, which enabled us to derive the abundances of alkali elements Na and K. Determinations of Na and K abundances in the atmospheres of

Table 6. CP stars investigated in this work.

KIC number	HD number	SpC (new)
	New Am stars	
3441230		kA2hA5mF0 V Am
5199439	225365	kA3hA5mA5 (IV)s Am:
5200084	225410	kA3hA6mF1 (IV) Am
5633448	225463	kA3hA4mA7 V Am
6292398		kA3hA7mA7 V Am:
6292925		kA2.5hA3mA7 (IV) Am:
7767565	196995	kA5hA7mF1 IV Am
	Known Am stars	
8323104	188911	kA2.5hA6mA7 (IV) Am
8703413	187254	kA3hA5mA9 (IV)s Am
9117875	190165	kA3hF0.5mF3 (III) Am
9147002	180237	kA3hA5mF3 V Am
9204718	176843	kA3hA9mF1 (IV) Am
	Am stars in SB2 systems	
8112039	187091	kA3hA5mA5 (IV)s Am:
4660665		kA3hA5mA5 IV Am:
6865077		kA3hA8mA6 (IV) Am
8692626		kA2hA4mA6 (IV) Am:
10616138		kA3hA6mA7 (IV)s Am:
	Ap star	
4768731	225914	A5 Vp (SrCrEu)
	λ Boo stars	
9828226		hA2kA0mB9 Vb.
5724440	187234	F0 Vnn weak met (A5)

Am stars are rare (Takeda et al. 2012), but important for establishing the theory explaining the chemical abundance peculiarities of A stars. The effective temperature of KIC 9117875, at 7300 K, is low in comparison with other Am stars in our sample. The star falls among the γ Dor stars in the $T_{\rm eff} - \log g$ diagram, but it is not a γ Dor star (see Section 7). The fifth known Am star, KIC 9147002 was previously classified as an A2p star by Bertaud (1960). Its abundance pattern is typical of Am stars, with a significant Sc underabundance and strong overabundances of heavy elements. The Am stars KIC 8703413, 9117875 and 9204718, were also studied by Catanzaro & Ripepi (2014). Their results are in agreement with the values obtained here, within the errors.

Six newly discovered Am stars are KIC 3441230, 5199439, 5200084, 5633448, 6292398, and 6292925. These have low $v \sin i$ and abundance patterns typical of Am stars. A seventh Am star is KIC 7767565, of spectral type kA5hA7mF1 IV, whose chemical abundances are not typical, because Ca and Sc are overabundant. This star has a moderate $v \sin i$ of 64 ± 3 km s^{-1}.

KIC 8112039 is a highly eccentric binary, also known as KOI-54 (Welsh et al. 2011; Burkart et al. 2012). Welsh et al. (2011) analysed the high-resolution spectrum taken in quadrature and determined atmospheric parameters of both components, finding $T_{{\rm eff}A}$ and $T_{{\rm eff}B}$ equal to 8500 and 8800 K, and surface gravities $\log g = 3.8$ and 4.1, respectively. Both stars appeared to be metal-rich, with [Fe/H] $= 0.4 \pm 0.2$ dex. They also determined low $v \sin i$ values for the components, at 7.5 and 4.5 km s^{-1}. The spectrum investigated in this paper was taken in conjunction, so that the lines of both stars overlap. From the analysis of our spectrum we derived $T_{\rm eff} = 8400$ K, $\log g = 3.7$ dex, [Fe/H] $= 0.0 \pm 0.13$ dex, and $v \sin i = 8 \pm 1$ km s^{-1}.

Four other stars were classified as Am stars and belong to SB2 binary systems: KIC 4660665, KIC 6865077, KIC 8692626, and

Downloaded from http://mnras.oxfordjournals.org/ at The Library on May 18, 2016

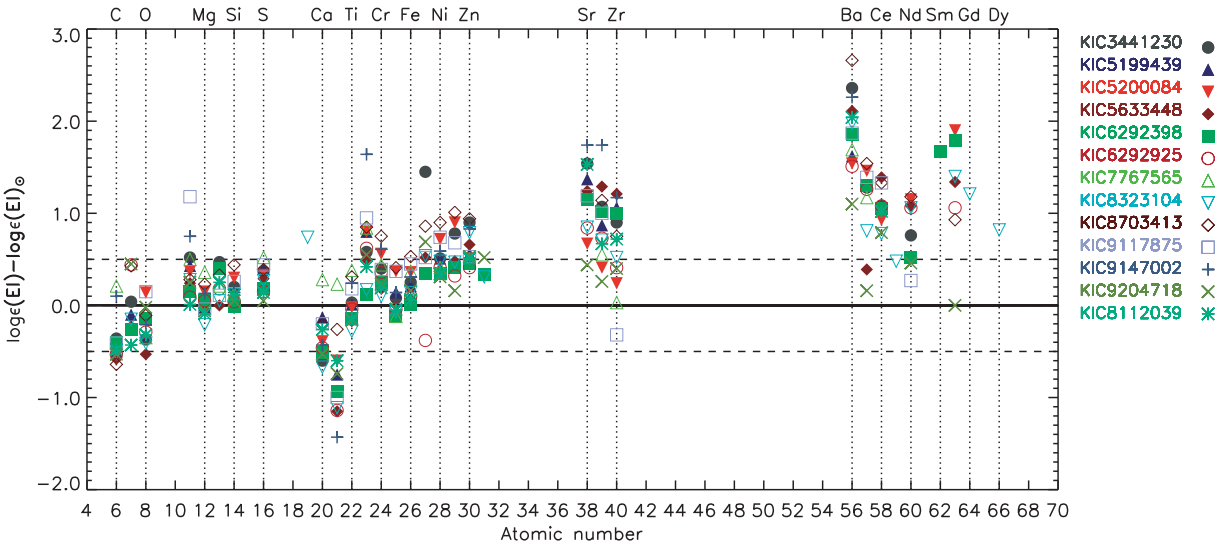

Figure 12. Chemical abundances of Am stars compared with the solar values (Asplund et al. 2009) as a function of the atomic number.

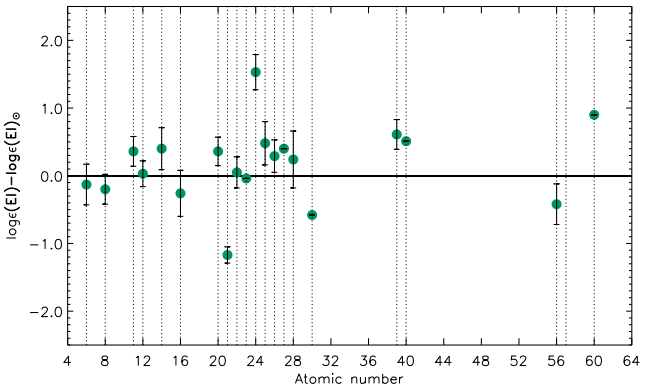

Figure 13. Chemical abundances of the Ap star KIC 4768731 compared with the solar values (Asplund et al. 2009) as a function of atomic number.

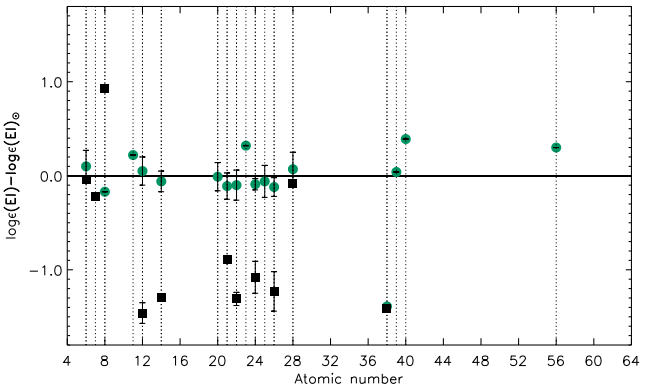

Figure 14. Obtained chemical abundances of the suspected λ Boo stars KIC 5724440 (filled circles) and KIC 9828226 (filled squares) compared with the solar values (Asplund et al. 2009) as a function of atomic number.

KIC 10616138. These stars, together with KIC 8112039, will be analysed in a forthcoming paper (Catanzaro et al., in preparation).

The only Ap star in our sample, KIC 4768731, has the spectral type A5 Vp (SrCrEu). According to Mason et al. (2001), the star is the primary of a visual binary with a separation of about 12 arcsec with $V = 9.19$ mag (primary) and 12.00 mag (secondary). Previously, KIC 4768731 was classified as an A7 star (see Table 2), without indication of chemical peculiarity. The chemical pattern of KIC 4768731 is typical for Ap (SrCrEu) stars, with significant overabundances of Cr and Sr (see Fig. 13). All Fe-peak elements, except for Sc, V, and Zn, are overabundant. Additionally, KIC 4768731 was discovered as a rapidly oscillating (roAp) star (Smalley et al., in preparation). Detailed spectral analysis of Ap stars requires taking into account stratification of the elements in their atmospheres. This effect has a substantial impact on spectral lines, so atmospheric parameters determined here from the ionization and excitation equilibria and wings of hydrogen lines can be incorrect. Results of spectral analysis with stratification of chemical elements for KIC 4768731 will be presented by Niemczura, Shulyak et al. (in preparation).

We classified two stars as probable λ Boo stars (Fig. 14). The spectral type obtained for KIC 9828226 is hA2kA0mB9 Vb. Its hydrogen lines are very broad, the metal lines are weak, and the magnesium Mg II 4481 line is especially weak when compared with the metal line type. The star has $v \sin i = 88 \pm 9$ km s^{-1}. For KIC 5724440 was given the spectral type F0 Vnn (weak met (A5)). Its hydrogen lines are broad and shallow – typical for a rapid rotator – and are consistent with an F0 spectral type, whereas its metal lines are weak and are similar in strength to the A5 standard HD 23886. The Ca II K line is broad but shallow, having the depth of the A3 V standard but the width of the A7 V standard. The moderate resolution spectrum of this star was analysed by Catanzaro et al. (2011), who indicated a problem with the effective temperature determination from Balmer lines. This problem was also noticed in this paper. The Mg II 4481 in the spectrum of KIC 5724440 is weaker than in the spectrum of a normal star with the same atmospheric parameters. The iron-peak elements and especially Sr are slightly underabundant. This supports the λ Boötis classification of this star.

7 DISCUSSION AND CONCLUSIONS

We analysed high-resolution HERMES/Mercator spectra of 117 A and F stars collected during the spectroscopic campaign of *Kepler* stars. Spectral classification showed that our sample consists mostly of non-evolved stars of luminosity types V to IV and revealed 20 CP stars of Am, Ap (CrSrEu), and λ Boötis types. These peculiarities were confirmed by detailed investigation of the stellar spectra. Nine

Downloaded from http://mnras.oxfordjournals.org/ at The Library on May 18, 2016

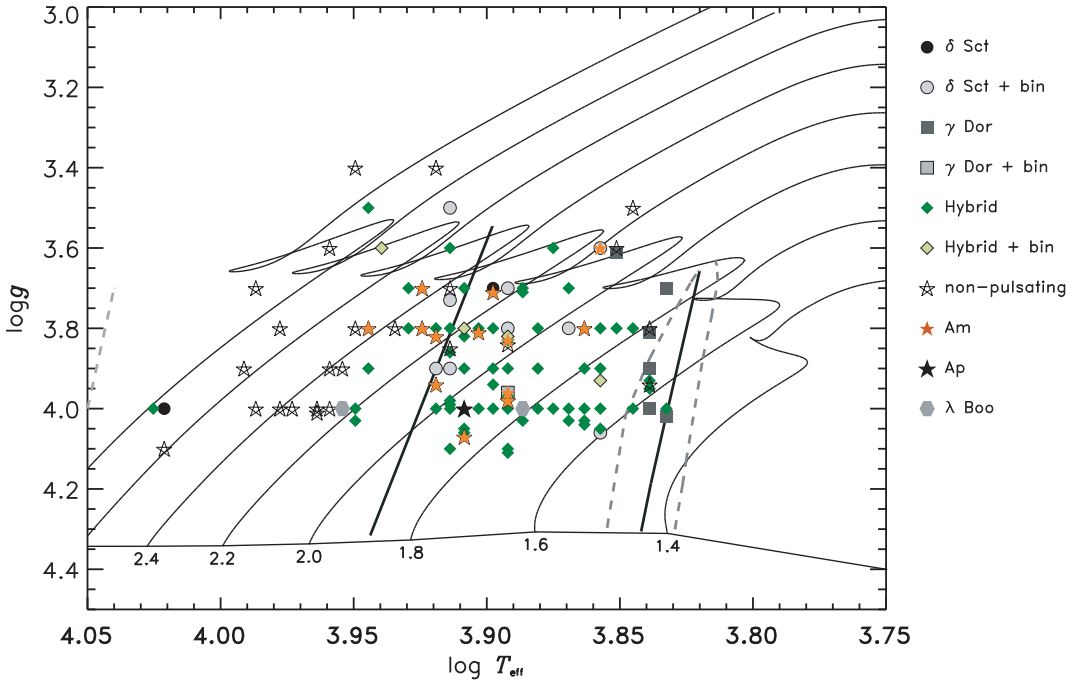

Figure 15. log $T_{\rm eff}$ – log g diagram for the stars analysed in this paper. Stars identified as single δ Sct are indicated by filled circles, δ Sct in a binary system as open circles, single γ Dor as filled squares, γ Dor in binary systems as light blue squares. Single stars with hybrid pulsations are plotted as filled diamonds, whereas hybrid stars in binary systems are open diamonds. Non-pulsating stars (including Am objects) are shown as stars.

new CP stars were found, of which six were Am, one was Ap, and two were λ Boo stars.

The atmospheric parameters, i.e. $T_{\rm eff}$, log g, $\xi_{\rm t}$, abundances of chemical elements, and $v \sin i$ for all stars were determined by using spectral synthesis. The atmospheric parameters were compared with the values taken from the KIC and those determined from SED fitting. Like the results reported by Tkachenko et al. (2013b) and Lehmann et al. (2011), the KIC values of effective temperatures were found to be lower than the spectroscopic ones for stars with $T_{\rm eff} \gtrsim 7500$ K. One of the reasons for these differences is probably the use of incorrect interstellar reddening when estimating the KIC temperatures. The $E(B-V)$ values from the KIC were compared with the spectroscopic values determined from interstellar Na D_2 lines. For $T_{\rm eff}$ higher than 7500 K, the differences $E(B-V)$(Na) − $E(B-V)$(KIC) increase. The spectroscopic effective temperatures derived from iron and Balmer lines are in good agreement with values obtained from SED fitting. For most stars, the surface gravities determined from iron lines and taken from the KIC are consistent to ±0.2 dex. There is a positive correlation between the differences of iron abundances determined from spectroscopy and taken from KIC and log ϵ(Fe). The same trend was noticed by Tkachenko et al. (2013b). This suggests that the KIC iron abundances of metal-weak stars are systematically overestimated, whereas iron abundances of metal-strong stars are underestimated. The obtained microturbulence velocities follow the trend presented by Landstreet et al. (2009) and are smaller towards higher effective temperatures. The obtained values of $v \sin i$ range from 8 to about 280 km s^{-1} with the average equal to 134 km s^{-1}, which is typical for A and early F stars.

The atmospheric parameters determined in this work are very important as input ingredients for further seismic modelling. We analysed A and F stars, so our sample contains pulsating δ Sct, γ Dor, and hybrid stars. To find out if the obtained atmospheric parameters of the stars are consistent with theoretical instability strips in this part of the H-R diagram, we performed an analysis of the *Kepler* data for all stars investigated here. We used the corrected light curves available through the MAST[11] data base. We considered all the long cadence data available for a given star. If necessary, short cadence data were used to verify our classification. The *Kepler* data from each quarter were shifted to have the same mean level and all quarters were merged. For some stars, it was necessary to remove the trends from each quarter separately. Then, we visually examined all light curves, the frequency spectra, and detected frequencies to identify candidate δ Sct, γ Dor, hybrid, and other types of variability. The results of our initial classification are presented in the last column of Table 2. We classified 15 stars as δ Sct, 13 as γ Dor, and 71 as δ Sct/γ Dor hybrid stars. In this paper, all objects for which we can find frequencies typical for δ Sct and γ Dor stars are termed hybrid. Moreover, we found 14 pulsating stars in binary systems, including eclipsing binaries, and 30 stars which do not show pulsations (these stars were discussed in detail by Murphy et al. 2015). The spectroscopic parameters provided here were critical for assigning locations of the non-pulsators with respect to the δ Sct instability strip. Here we only mention that light curves of the stars belonging to the latter group show variability resulting from rotation and spots on the surfaces of these stars and/or from binarity (see Table 2).

All of the stars investigated are shown in a log $T_{\rm eff}$ – log g diagram (Fig. 15). We added evolutionary tracks, calculated with time-dependent convection (Grigahcène et al. 2005), for stars having [Fe/H] = 0.0 and $\alpha_{\rm MLT} = 2.0$ covering a range of masses from 1.4 to 2.8 $M_\odot$. The stars are plotted with different symbols depending on the type of pulsations, type of chemical peculiarity and other characteristics. As we can see in Fig. 15, non-pulsating stars are situated inside and on the blue edge of the δ Sct instability strip. Most

[11] https://archive.stsci.edu/kepler/

Downloaded from http://mnras.oxfordjournals.org/ at The Library on May 18, 2016

Am stars are located inside the instability strip. Most hybrid stars are located inside or close to the blue edge of the δ Sct instability strip. The exceptions are KIC 12736056 and 8489712, whose effective temperatures are too high for hybrid δ Sct/γ Dor stars. The same applies for KIC 4056136, classified as a δ Sct star, KIC 11180361, showing variability typical for hybrid stars and binarity, and for KIC 6292398, for which we found γ Dor frequencies and evidence for binarity. All these stars need further investigation to verify the possibility of contamination by another star. The frequency analysis of the *Kepler* data revealed 31 stars with low-frequency peaks, which we attribute to binarity. For these stars, lines from only one star are present in the spectrum and we see δ Sct and/or γ Dor frequencies in the *Kepler* data.

We investigated 13 Am type stars, of which seven are newly discovered. Most of them show only the variability typical for stars in binary systems or due to rotation and spots. Only three stars are possible pulsators. KIC 6292398 has a frequency pattern found in γ Dor stars and binarity, KIC 7767565 is probably also a γ Dor star, and KIC 9204718 shows frequencies typical of binarity, rotational changes and δ Sct pulsations. The *Kepler* photometric data for these stars need to be analysed in detail.

We have also investigated a possible relationship between metallicities or chemical peculiarities and the hybrid pulsations. The first δ Sct/γ Dor hybrid, HD 8801, was discovered by Henry & Fekel (2005) and classified as an Am star. This classification was confirmed by Neuteufel, Weiss & Handler (2013). Hareter et al. (2011) analysed the spectra of two other hybrid stars, HD 114839 and BD $+18^\circ$ 4914, discovered with MOST photometry by Rowe et al. (2006) and King et al. (2006), respectively. The evolved star BD$^\circ$ +18 4914 has an abundance pattern typical for an Am star, but the less evolved star HD 114839, previously classified in the literature as a mild Am star, does not show any peculiarity. For 58 hybrid candidates investigated here the spectral analyses do not indicate any peculiarity.

ACKNOWLEDGEMENTS

We are grateful to the anonymous referee for their thorough examination of this paper. EN acknowledges support from Fundaçao para a Ciência e a Tecnologia (FCT) through the grant 'Cooperaç ao Cientica e Teccnologica FCT/Polonia 2011/2012 (Proc. 441.00 Polonia)' funded by FCT/MCTES, Portugal and the support from 1007/S/IAs/14 funds. This work was supported by NCN grant 2011/01/B/ST9/05448. DD would like to acknowledge the NSC grant no. 2011/01/N/ ST9/00400. Calculations were carried out in the Wrocław Centre for Networking and Supercomputing (http://www.wcss.pl), grant no. 214. This research was supported by the Australian Research Council. Funding for the Stellar Astrophysics Centre is provided by the Danish National Research Foundation (grant agreement no. DNRF106). The research is supported by the ASTERISK project (ASTERoseismic Investigations with SONG and Kepler) funded by the European Research Council (grant agreement no. 267864). KU acknowledges support from the Spanish National Plan of R&D for 2010, project AYA2010-17803. The research leading to these results has received funding from the European Research Council under the European Community's Seventh Framework Programme (FP7/20072013)/ERC grant agreement no. 227224 (PROSPERITY). This publication makes use of data products from the Two Micron All Sky Survey, which is a joint project of the University of Massachusetts and the Infrared Processing and Analysis Center/California Institute of Technology, funded by the National Aeronautics and Space Administration and the National Science Foundation. MB is a FRS-FNRS postdoctoral researcher in Belgium. AP acknowledges support from NCN grant no. 2011/03/B/ST9/02667. PIP is a postdoctoral fellow of the Fund for Scientific Research (FWO), Flanders, Belgium. SB is supported by the Foundation for Fundamental Research on Matter (FOM), which is part of the Netherlands Organization for Scientific Research (NWO).

REFERENCES

Abt H. A., 2000, AJ, 544, 933
Abt H. A., 2009, AJ, 138, 28
Abt H. A., Hudson K. I., 1971, ApJ, 163, 333
Abt H. A., Morrell N. I., 1995, ApJS, 99, 135
Abt H. A., Moyd K. I., 1973, ApJ, 182, 809
Antoci V. et al., 2014, ApJ, 796, 118
Asplund M., Grevesse N., Sauval A. J., Scott P., 2009, ARA&A, 47, 481
Babel J., 1993, ASP Conf. Ser. Vol. 44, Diffusion Models for Magnetic Ap-Stars, Astron. Soc. Pac., San Francisco, CA, p. 458
Balona L. A., 2014, MNRAS, 437, 1476
Balona L. A., Dziembowski W., 2011, MNRAS, 417, 591
Balona L. A. et al., 2011, MNRAS, 414, 792
Bergemann M., Lind K., Collet R., Magic Z., Asplund M., 2012, MNRAS, 427, 27
Bertaud C., 1960, Journal des Observateurs, 43, 129
Bevington P. R., 1969, Data reduction and error analysis for the physical sciences. McGraw-Hill, New York
Bonaca A. et al., 2012, ApJ, 755, L12
Borucki W. J. et al., 2010, Science, 327, 977
Breger M., 2000, Balt Astron., 9, 149
Brown T. M., Latham D. W., Everett M. E., Esquerdo G. A., 2011, AJ, 142, 112
Burkart J., Quataert E., Arras P., Weinberg N. N., 2012, MNRAS, 421, 983
Cardelli J. A., Clayton G. C., Mathis J. S., 1989, ApJ, 345, 245
Carnochan D. J., 1979, Bull. Inf. CDS, 17, 78
Castelli F., Hubrig S., 2004, A&A, 425, 263
Catanzaro G, Leone F., Dall T. H., 2004, A&A, 425, 641
Catanzaro G., Ripepi V., 2014, MNRAS, 441, 1669
Catanzaro G. et al., 2011, MNRAS, 411, 1167
Dommanget J., Nys O., 2002, Catalog of components of double & multiple stars
Donati J.-F., Semel M., Carter B. D., Rees D. E., Collier Cameron A., 1997, MNRAS, 291, 658
Droege T. F., Richmond M. W., Sallman M., 2006, PASP, 118, 1666
Evans D. W., Irwin M. J., Helmer L., 2002, A&A, 395, 347
Fabricius C., Høg E., Makarov V. V., Mason B. D., Wycoff G. L., Urban S. E., 2002, A&A, 384, 180
Floquet M., 1975, A&A, 21, 25
Folsom C. P., Wade G. A., Bagnulo S., Landstreet J. D., 2007, MNRAS, 376, 361
Fossati L., Bagnulo S., Landstreet J., Wade G., Kochukhov O., Monier R., Weiss W., Gebran M., 2008, A&A, 483, 891
Fossati L., Ryabchikova T., Shulyak D. V., Haswell C. A., Elmasli A., Pandey C. P., Barnes T. G., Zwintz K., 2011, MNRAS, 417, 495
Gebran M., Monier R., 2008, A&A, 483, 567
Gebran M., Monier R., Richard O., 2008, A&A, 479, 189
Gebran M., Vick M., Monier R., Fossati L., 2010, A&A, 523, AA71
Gebran M., Monier R., Royer F., Lobel A., Blomme R., 2014, psce.conf, 193
Gray R. O., 1985, J. R. Astron. Soc. Can., 79, 237
Gray D. F., 2005, The Observation and Analysis of Stellar Photospheres. Cambridge University Press, Cambridge
Gray R. O., Corbally C. J., 2009, Stellar Spectral Classification. Princeton University Press, Princeton, NJ
Grigahcène A., Dupret M.-A., Gabriel M., Garrido R., Scuflaire R., 2005, A&A, 434, 1055

Downloaded from http://mnras.oxfordjournals.org/ at The Library on May 18, 2016

Grigahcène A. et al., 2010, ApJ, 713, L192
Gulliver A. F., Hill G., Adelman S. J., 1994, ApJ, 429, 81
Handler G., 2009, AIP Conf. Ser., 1170, 403
Hareter M., Fossati L., Weiss W., Suárez J. C., Uytterhoeven K., Rainer M., Poretti E., 2011, ApJ, 743, 153
Heckmann O., Dieckvoss W., 1975, AGK3 catalogue
Henry G. W., Fekel F. C., 2005, AJ, 129, 2026
Howarth I. D., 1983, MNRAS, 203, 301
Huber D. et al., 2014, ApJS, 211, 2 (H2014)
Hubrig S. et al., 2005, A&A, 440, L37
Høg E. et al., 1997, A&A, 323, L57
Kaye A. B., Handler G., Krisciunas K., Poretti E., Zerbi F. M., 1999, PASP, 111, 840
King H. et al., 2006, Commun. Asteroseismology, 148, 28
King J. R., 1994, MNRAS, 269, 209
Kjeldsen H., Christensen-Dalsgaard J., Handberg R., Brown T. M., Gilliland R. L., Borucki W. J., Koch D., 2010, Astron. Nachr., 331, 966
Kochukhov O., Makaganiuk V., Piskunov N., 2010, A&A, 524, A5
Kochukhov O. et al., 2015, A&A, 574, AA79
Koppen J., Vergely J. L., 1998, MNRAS, 299, 567
Kurtz D. W., Elkin V. G., Cunha M. S., Mathys G., Hubrig S., Wolff B., Savanov I., 2006, MNRAS, 372, 286
Kurtz D. W, Freyhammer L. M., Elkina V. G., Mathys G., 2007a, AIP Conf. Proc., 948, 249
Kurtz D. W, Elkin V. G., Mathys G., van Wyk F., 2007b, MNRAS, 381, 1301
Kurtz D. W., Saio H., Takata M., Shibahashi H., Murphy S. J., Sekii T., 2014MNRAS, 444, 102
Kurucz R. L., 1993a, Kurucz CD-ROM 13.SAO, Cambridge, USA
Kurucz R. L., 1993b, Kurucz CD-ROM 18.SAO, Cambridge, USA
Kurucz R. L., 2011, Can. J. Phys., 89, 417
Lampens P. et al., 2012, Astron. Nachr., 333, 975
Landstreet J. D., Kupka F., Ford H. A., Officer T., Sigut T. A. A., Silaj J., Strasser S., Townshend A., 2009, A&A, 503, 973
Lehmann H. et al., 2011, A&A, 526, A124
Marques J. P. et al., 2013, A&A, 549, A74
Marshall D. J., Robin A. C., Reylé C., Schultheis M., Picaud S., 2006, A&A, 453, 635
Mashonkina L., 2011, mast.conf, 314
Mason B. D., Wycoff G. L., Hartkopf W. I., Douglass G. G., Worley C. E., 2001, AJ, 122, 3466
Mendoza E. E., 1974, Rev. Mexican Astron. Astrophys., 1, 175
Michaud G., Richer J., 2013, EAS Publ. Ser. Vol., 63, 199
Molenda-Żakowicz J., Latham D. W., Catanzaro G., Frasca A., Quinn S. N., 2011, MNRAS, 412, 1210
Monet D. G. et al., 2003, AJ, 125, 984
Moravveji E., Guinan E. F., Shultz M., Williamson M. H., Moya A., 2012, ApJ, 749, 74
Mosser B. et al., 2012, A&A, 548, A10
Munari U., Zwitter T., 1997, A&A, 318, 26
Murphy S. J., 2014, PhD thesis, Univ. Central Lancashire
Murphy S. J., Bedding T. R., Niemczura E., Kurtz D. W., Smalley B., 2015, MNRAS, 447, 3948
Neuteufel R., Weiss W., Handler G., 2013, Astron. Nachr., 334, 638
Niemczura E., Połubek G., 2006, in Fletcher K., Thompson M., eds, ESA SP-624, Proc. SOHO 18/GONG 2006/HELAS I, Beyond the Spherical Sun. Sheffield, UK, p. 120
Niemczura E., Morel T., Aerts C., 2009, A&A, 506, 213
Noci G., Pomilia A., Ortolani S., 1986, in Zeilik M., Gibson D. M., eds, Lecture Notes in Physics, Vol. 254, Springer-Verlag, Berlin, Heidelberg, New York, p. 130
Paunzen E., Iliev I. K., Fossati L., Heiter U., Weiss W. W., 2014, A&A, 567, AA67
Przybilla N., Butler K., Becker S. R., Kudritzki R. P., Venn K. A., 2000, A&A, 359, 1085
Raskin G. et al., 2011, A&A, 526, A69
Richard O., 2005, EAS Publ. Ser. Vol. 17, p. 43
Rowe J. F. et al., 2006, Commun. Asteroseismology, 148, 34
Royer F., 2009, The Rotation of Sun and Stars, Lecture Notes in Physics, Vol. 765. Springer, Berlin, p. 207
Royer F., Zorec J., Gómez A. E., 2007, A&A, 463, 671
Royer F. et al., 2012, SF2A-2012, Proc. Ann. Meeting French Soc. Astron. Astrophys. p. 389
Royer F. et al., 2014, A&A, 562, A84
Rufener F., 1999, VizieR OnlineData Catalog, II/169
Ryabchikova T., 2014, psce.conf, 220
Ryabchikova T., Leone F., Kochukhov O., 2005, A&A, 438, 973
Saio H., Kurtz D. W., Takata M., Shibahashi H., Murphy S. J., Sekii T., Bedding T. R., 2015, MNRAS, 447, 3264
Sbordone L., 2005, Mem. Soc. Astron. Ital. Suppl., 8, 61
Seaton M. J., 1979, MNRAS, 187, 73
Skrutskie M. F. et al., 2006, AJ, 131, 1163
Smalley B., 2004, in Zverko J., Ziznovsky J., Adelman S. J., Weiss W. W., eds, Proc. IAU Symp., 224, Observations of convection in A-type stars. Cambridge Univ. Press, Cambridge, p. 131
Takeda Y., 1995, PASJ, 47, 287
Takeda Y., Han I., Kang D. I., Lee B. C., Kim K. M., 2008, J. Korean Astron. Soc., 41, 83
Takeda Y., Kang D. I., Han I., Lee B. C., Kim K. M., 2012, PASJ, 64, 38
Talon S., Richard O., Michaud G., 2006, ApJ, 645, 634
Tkachenko A., Van Reeth T., Tsymbal V., Aerts C., Kochukhov O., Debosscher J., 2013a, A&A, 560, A37
Tkachenko A., Lehmann H., Smalley B., Uytterhoeven K., 2013b, MNRAS, 431, 3685
Trampedach R., Stein R. F., 2011, ApJ, 731, 78
Turcotte S., 2003, in Balona L. A., Henrichs H. F., Medupe R., eds, ASP Conf. Ser. Vol. 305, Magnetic Fields in O, B and A Stars: Origin and Connection to Pulsation, Rotation and Mass Loss. Astron. Soc. Pac., San Francisco, p. 199
Uytterhoeven K., 2014, in Determination of Atmospheric Parameters of B-, A-, F- and G-Type Stars, Springer Series: GeoPlanet: Earth and Planetary Sciences, Springer International Publishing, p. 1
Uytterhoeven K. et al., 2010, Astron. Nachr., 331, 993
Uytterhoeven K. et al., 2011, A&A, 534, A125
Venn K. A., Lambert D. L., 1990, ApJ, 363, 234
Welsh W. F. et al., 2011, ApJS, 197, 4

SUPPORTING INFORMATION

Additional Supporting Information may be found in the online version of this article:

supplementary_material.tar.gz (http://mnras.oxfordjournals.org/lookup/suppl/doi:10.1093/mnras/stv528/-/DC1).

Please note: Oxford University Press are not responsible for the content or functionality of any supporting materials supplied by the authors. Any queries (other than missing material) should be directed to the corresponding author for the article.

[1]*Instytut Astronomiczny, Uniwersytet Wrocławski, Kopernika 11, PL-51-622 Wrocław, Poland*
[2]*Sydney Institute for Astronomy (SIfA), School of Physics, University of Sydney NSW 2006, Australia*
[3]*Stellar Astrophysics Centre, Department of Physics, and Astronomy, Aarhus University, DK-8000 Aarhus C, Denmark*
[4]*Astrophysics Group, Keele University, Staffordshire, ST5 5BG, UK*
[5]*Instituto de Astrofisica de Canarias, E-38205 La Laguna, Tenerife, Spain*
[6]*Universidad de La Laguna, Departamento de Astrofisica, E-38206 La Laguna, Tenerife, Spain*
[7]*Thüringer Landessternwarte Tautenburg (TLS), Sternwarte 5, D-07778 Tautenburg, Germany*
[8]*Jeremiah Horrocks Institute, University of Central Lancashire, Preston PR1 2HE, UK*

Downloaded from http://mnras.oxfordjournals.org/ at The Library on May 18, 2016

[9]*INAF-Osservatorio Astrofisico di Catania, Via S. Sofia 78, I-95123, Catania, Italy*
[10]*Instituut voor Sterrenkunde, KU Leuven, Celestijnenlaan 200D, B-3001, Leuven, Belgium*
[11]*Department of Astrophysics, IMAPP, Radboud University Nijmegen, PO Box 9010, NL-6500 GL Nijmegen, the Netherlands*
[12]*Institut d'Astrophysique et de Géophysique, Université de Liège, Allée du 6 Août 17, B-4000 Liège, Belgium*
[13]*Royal observatory of Belgium, Ringlaan 3, B-1180 Brussel, Belgium*
[14]*University of Geneva, Department of Astronomy, Chemin des Maillettes, 51, Sauverny, CH-1290, Switzerland*
[15]*Instituto de Astrofísica e Ciências Espaciais and Faculdade de Ciências, Universidade do Porto, Rua das Estrelas, PT4150-762 Porto, Portugal*
[16]*Astronomical Observatory, Adam Mickiewicz University, ul. Słoneczna 36, PL-60-286 Poznań, Poland*
[17]*Centrum Badań Kosmicznych, Polska Akademia Nauk, Kopernika 11, 51-622 Wrocław*

This paper has been typeset from a TEX/LATEX file prepared by the author.

Downloaded from http://mnras.oxfordjournals.org/ at The Library on May 18, 2016